

Motion of CMS structures during Magnet Cycles and Stability Periods from 2008 to 2013 as observed by the Link Alignment System

P. Arce, J.M. Barcala, E. Calvo, A. Ferrando*, M.I. Josa, A. Molinero,
J. Navarrete and J.C. Oller
CIEMAT (Madrid, Spain)

J. Brochero, A. Calderón, M.G. Fernández, G. Gómez, F.J. González-Sánchez, C.
Martínez-Rivero, F. Matorras, T. Rodrigo, L. Scodellaro, M. Sobrón, I. Vila
and A.L. Virto

Instituto de Física de Cantabria, CSIC–University of Cantabria (Santander, Spain)
J. Fernández

University of Oviedo (Oviedo, Spain)

P. Raics, Zs. Szabó, Z. Trócsnyi, B. Ujvári and Gy. Zilizi
University of Debrecen, Institute of Experimental Physics (Debrecen, Hungary)

N. Béni, G. Christian, J. Imrek, J. Molnar, D. Novak, J. Pálinkás, G. Székely
and Z. Szillási

Institute of Nuclear Research ATOMKI (Debrecen, Hungary)

G.L. Bencze and G. Vestergombi

KFKI Research Institute for Particle and Nuclear Physics (Budapest, Hungary)

M. Benettoni, F. Gasparini, F. Montecassiano, M. Rampazzo and M. Zago
Dipartimento di Fisica dell'Università di Padova e Sezione dell'INFN (Padova, Italy)

A. Benvenuti

Dipartimento di Fisica dell'Università di Bologna e Sezione dell'INFN (Bologna, Italy)

H. Reithler

Physikalisches Institut IIIA, RWTH Aachen University (Aachen, Germany)

P. Ruiz-Árbol

Swiss Federal Institute of Technology Zürich (Zürich, Switzerland)

Abstract

Magnet Cycles and Stability Periods of the CMS Experiment are studied with the Alignment Link System data recorded along the 2008 to 2013 years of operation. The motions of the mechanical structures due to the magnetic field forces are studied and the mechanical stability of the detector during the physics data taking periods is verified.

(To be submitted to Nucl. Instr. and Methods A)

Keywords: CMS, alignment, stability.

* Corresponding author.

E-mail address: antonio.ferrando@ciemat.es

1. Introduction

A major part of the Compact Muon Solenoid detector (CMS) [1-4] is a powerful muon spectrometer [3] for the identification and measurement of muons in a very wide energy range, from few GeV up to several TeV. Disregarding the low angle calorimeters, CMS has a cylindrical symmetry around the LHC beam pipe, an overall diameter of 15 m, a total length of 21.6 m and weighs 12.5 kt (mainly iron). At its heart, a 13 m long, 6 m inner diameter superconducting solenoid [2] provides a 3.8 T field along the beam axis and a bending power of about 12 Tm in the transverse plane. The return field is captured through 1.5 m of iron layers, allowing four muon stations to be integrated, both in the barrel and in the end-cap regions, to ensure full geometrical coverage.

The accuracy required in the position of the muon chambers is driven by the resolution demanded in the momentum measurement of high energy muons. CMS is designed to achieve a combined (Muon System [3] and Tracker [4]) momentum resolution of 0.5 – 1% for $p_T \approx 10$ GeV, 1.5 – 5% for $p_T \approx 100$ GeV and 5 – 20% for $p_T \approx 1$ TeV for the region $|\eta| < 2.4$. This design accuracy requires the knowledge of the position of the chambers with a precision *comparable* to their resolution.

Several simulation studies were performed [5] in order to quantify the importance of muon chamber alignment in the momentum resolution. For the most important coordinate from the physics point of view, ($R\Phi$), the alignment system should reconstruct the position of the chambers within 150 – 300 μm for MB1 – MB4 and within 75 – 200 μm for ME1 – ME4. The tighter constraints correspond to MB1 and ME1 since the magnetic bending in the yoke is reversed with respect to the inner magnetic field and hence the largest bending is to be measured in the first stations. Since these stations are located at the border of the magnet they allow, in combination with the Tracker hits, to exploit the full bending space in the CMS experiment.

When CMS is in operation, the movements and deflections of the muon spectrometer may exceed 100 μm . To monitor these movements, CMS is instrumented with an opto-mechanical alignment system that performs a continuous and precise measurement of the relative position of the muon chambers amongst themselves as well as the position of the muon spectrometer with respect to the tracker, assumed to be a rigid body. The information provided by the alignment system is used for the off-line track reconstruction.

In a previous document [6] the alignment system was presented and, using the first data taken by the Link Alignment System during the two phases of the 2006 Magnet Test and Cosmic Challenge, the effects of the ramp up and down in magnetic field were studied. It was shown that the Link system could obtain geometrical reconstructions of relative spatial locations and angular orientations between the muon chambers and the tracker body with a resolution better than 150 μm for distances and about 40 μrad for angles.

The structural equilibrium was also investigated [7]. Using data from the years 2008 and 2009, it was found that once the magnetic field intensity reaches 3.8 T, provided that the current in the coils remains unaltered, the mechanical structures reach equilibrium within the first 24 h. By structural equilibrium is understood that any further displacement in any direction (axial or radial) will remain within the short distance sensors resolution: ~ 40 μm and any rotation will be smaller than the tilt sensors resolution: ~ 40 μrad . Periods satisfying these constraints will be called *Stability Periods*.

However, and as also explained in Ref. [7], a long term monitoring of 2010 link data showed an apparent exception to the observed structural equilibrium: during the periods at constant $B = 3.8\text{T}$ and after the first 24 hours, the central part of the $YE_{\pm 1}$ endcap structures seemed to have an *accordion-like* motion of amplitude in the range $200 - 250\ \mu\text{m}$, towards and away the CMS geometrical centre.

In the present study the *Magnet Cycles* (the elapsed time between the switching of the current in the coils on and off) and the *Stability Periods* (up to 4T in the first year of operation and at 3.8 T in the subsequent years) during this six-year survey are identified and investigated. Physics data are taken during the *Stability Periods*.

The document presents a summary of the CMS Link Alignment monitoring of the relative motions of mechanical structures during the full period from 2008 to 2013. The study includes the influence of eventual temperature changes in the calculation of the relative distances between the endcap disks of the forward muon chambers and the central tracker with the aim of finding a possible explanation to the recorded motions that, in Ref. [7], are detected surpassing the $40\ \mu\text{m}$ resolution.

This article is organized as follows: a short description of the CMS Alignment System is given in section 2. Magnet Cycles and Stability Periods are presented in Section 3. In Section 4 the monitoring of variables assumed to be mechanically stable during the physics data taking periods prove that the stability requirements are respected all along the six years of operation. The results of the monitoring of the distances between the Link Disks and its corresponding Alignment Rings, $Z(\text{LD-AR})$, during the various Magnets Cycles along the 2008-2013 operations, are presented in Section 5. Section 6 is devoted to the study of the relative $\Delta Z(\text{LD-AR})$ distances during the Stability Periods along these six years, with special emphasis in the analysis of the monitored temperature in the volume between the Link Disks and the Alignment Rings and the discussion of the correlation between both quantities. Finally, summary and conclusions are given in Section 7.

2. The CMS Alignment System

A longitudinal view of one quadrant of the CMS experiment showing the various detectors is given in Fig. 1. Different muon detection technologies are employed for the central and the endcap regions, due to the different conditions of the magnetic field in terms of intensity and homogeneity. In the barrel region, surrounding the coil of the solenoid, four concentric stations of drift tube (DT) chambers (named MB1 to MB4), are inserted in the five wheels that constitute the return iron yoke. A muon chamber is built of three superlayers. Each superlayer in turn is made of four layers of drift cells, being the drift cell the basic detection unit. Drift times are translated into local space positions with a single hit resolution of $250\ \mu\text{m}$. Superlayers are arranged such that they measure the muon in two orthogonal coordinates: two superlayers measure the muon in the bending plane and the third superlayer measures it along the beam axis direction. The mechanical design of a drift chamber is driven by the $100\ \mu\text{m}$ spatial precision requirement in the determination of the track position in the bending plane. Track segments are obtained by linear fits to the reconstructed hits in each coordinate. The DT chambers are subject to variable residual magnetic fields below 0.4 T for all the stations except for the innermost MB1 chambers closest to the endcaps, where the field reaches 0.8 T.

At both CMS endcap sides there are four layers of muon chambers, named ME1 to ME4. In the endcap regions the magnetic field is typically high and very

inhomogeneous due to its bending to feed the barrel yoke. In addition, at the level of the ME1 chambers the field intensity may be as high as 3 T. To cope with this and with the high particle fluxes in these regions, different gas ionization detectors called Cathode Strip Chambers (CSCs) are used for this region. The CSCs are multi-wire proportional chambers in which one cathode plane is segmented into strips running across wires, giving 2D information of the particle passage. Due to the intense magnetic field, the muon trajectories bend more in the vicinity of the first endcap station, where a higher precision is required (75 μm). For the rest of the chambers the necessary precision is about 150 μm .

Layers of Resistive Plate Chambers (RPCs), both in the barrel and in the endcaps, complement the muon spectrometer. They are used mainly for trigger purposes as their time resolution is better than 2 ns, although their hits may also participate in the muon track reconstruction. The RPCs are not aligned in CMS: they are assumed to be placed at their nominal positions within their spatial resolution of about 1 cm.

Typically, the total number of hits registered along a muon track is about 40. The muon momentum is measured through its bending in the transverse plane. The radius of curvature ρ and the momentum of the muon in the plane perpendicular to the magnetic field (p_T) are related by $\rho[\text{m}] = p_T[\text{GeV}]/0.3 \text{ B}[\text{T}]$. The radius of curvature is obtained from the measurement of the muon trajectory sagitta s , after traversing a distance d in the magnetic field, using the approximate expression $\rho = d^2/8s$. An error in the sagitta measurement results in an error in the momentum measurement.

The relative error in the sagitta measurement is $\delta s/s = \delta p_T/p_T$, proportional to $\sigma(s)p_T/d^2B$, where $\sigma(s)$ is the resolution in the sagitta measurement. The relative error in the momentum increases with the muon momentum and decreases linearly with the magnetic field and quadratically with the traversed distance.

A right-handed coordinate system is used in CMS, with the origin at the nominal interaction point (IP), the X-axis pointing to the centre of the LHC ring, the Y-axis pointing up (perpendicular to the LHC plane), and the Z-axis along the anticlockwise-beam direction. The polar angle Θ is measured from the positive Z-axis and the azimuthal angle Φ is measured in the XY-plane. The pseudorapidity is a geometrical variable defined as $\eta = -\ln[\tan(\Theta/2)]$.

At 3.8 T the solenoid induces an axial force of about 10,000 ton on the endcap iron yokes in the direction of the IP. Aluminium blocks, called Z-stops, are located between the endcap disks and the barrel region, as well as between the five barrel wheels, to prevent the different structures from being crushed into each other. The positions of the Z-stops are indicated in Fig. 1. While the barrel wheels suffer a small axial compression, the deformation of the endcap iron disks due to the magnetic forces and the resistance of the barrel Z-stops, sketched in Fig. 2, is very significant.

In order to meet the muon momentum resolution requirements mentioned above, CMS is instrumented with an Alignment System organised in three basic blocks:

- The Tracker alignment system [4] measures the relative position of the various tracker modules and monitors eventual internal deformations.
- The Muon (Barrel and Endcaps) alignment system [3] monitors the relative positions among the DT and CSC muon chambers.

- The Link System connects the position of the two muon subsystems, Barrel and Endcaps to the position of the tracker body and monitors the relative movements between them.

The Link System [8] is composed of several types of sensors supported by a series of independent reference rigid bodies which are individually calibrated and intercalibrated on special benches and measured by photogrammetry once installed in CMS. The position of the sensors define three alignment planes 60° apart, starting at $\Phi = 15^\circ$. Fig. 3 a) shows one of the Φ Link alignment planes where the three alignment subsystems can be seen. Each plane contains four independent alignment quadrants where the three systems are connected. The three Φ Link planes are also depicted on Fig. 3 b), where the CMS coordinate system is also indicated. A sketch of one quadrant of a Φ Link alignment plane with its instrumentation is shown in Fig. 4.

A distributed network of Amorphous Silicon Position Detectors (ASPDs) in each quadrant is connected by laser lines. An ASPD sensor [9-11] consists of two groups of 64 silicon micro-strips $408\ \mu\text{m}$ wide, with a pitch of $430\ \mu\text{m}$, oriented perpendicularly. Total active area is about $30 \times 30\ \text{mm}^2$.

The measured spatial resolutions of the reconstructed light spot on the sensor active area are $5.2 \pm 2.6\ \mu\text{m}$ and $5.1 \pm 2.4\ \mu\text{m}$ for the X- and Y-sensor coordinates, respectively [11].

Each of the 12 alignment quadrants use four laser light paths, one originating at the Tracker, two at the Endcap, and one at the Barrel region as indicated in Fig. 4, resulting in 48 laser paths, 24 on each side (positive or negative Z) of the CMS detector.

All laser-source collimators are housed in rigid carbon fibre structures called Alignment Rings (ARs), Modules for the Alignment of the Barrel (MABs) and Link Disks (LDs).

The ARs are annular structures attached to the Back Disks (BDs), the outermost, uninstrumented, Tracker Endcap discs. The LDs, annular structures as well, are suspended from the outer diameter of the YN1 iron disks of the endcap muon spectrometer by means of aluminium tubes attached to mechanical assemblies called Transfer Plates (TPs). MABs are mounted onto the barrel yoke elements.

The laser-ASPD measurement network is complemented by electrolytic tiltmeters for angular measurements with respect to the gravity, optical and mechanical proximity sensors for short distance measurements, aluminium tubes (longitudinal and radial profiles, labelled LP and RP on Fig. 4) for long distance measurements and magnetic probes and temperature sensors (not shown in Fig. 4).

The relative distance between LD and AR structures along the CMS Z coordinate is monitored at three different Φ positions ($\pm 75^\circ$, $\pm 195^\circ$ and $\pm 315^\circ$, the sign indicating the Z side) by Sakae potentiometers [12] located at the AR in contact with targets mounted on 3610 mm long Longitudinal Profiles attached to the LD. These six variables will be one of the main objects of the present study.

The relative Z distance between the TP and the ME/1/1 chamber is measured by a contact potentiometer installed in the TP touching a target situated on the top side of the ME/1/1 chamber (see Fig 4).

The rest of the relative distance measurements between CMS elements in a Φ quadrant monitor motions in the radial direction. The radial distance between LD and the MAB structures is done through several concatenated long and short distance measurements. First, the radial distance between LD and TP, the longest one monitored, it is measured using a 1977 mm long Radial Profile (RP in Fig. 4) instrumented with a

potentiometer located in its end closest to the LD. The relative displacement between the TP and the bottom side of the ME/1/2 chamber is also monitored using a contact potentiometer. The relative radial distance between the MAB and the outer side of the ME/1/2 chamber is monitored using a non-contact proximity sensor (Omron [13]) installed at the innermost part of each MAB structure. The sensor emitting/receiving head directs a laser light and receives the reflected light to/from a reflective target located on the outer region of the ME/1/2 chamber.

The combined uncertainty in the measurement of absolute positions is estimated to be about 300 μm . It includes the uncertainty in the length of the mechanical supports, the proximity sensor resolution/precision and the mounting uncertainty. Nevertheless, relative distance measurements, which are the relevant ones for this study, are only affected by the precision of the proximity sensors, $\sim 40 \mu\text{m}$.

All the alignment structures (ARs, LDs, TPs, and MABs) are instrumented with different models of tiltmeter sensors [14] which provide direct information on any changes in their orientations (small rotations/tilts). The precision of these sensors is of the order of 40 μrad [15]. With these devices, the Link Alignment System can monitor changes in Φ (azimuthal angle, rotations around the Z-axis) and Θ (polar angle, rotations around the X-axis) of the AR, BD, LD and TP structures. Tiltmeters located in the ARs and the BDs, are sensitive to rotations (Φ) and/or bending (Θ) of the Tracker body. In the case of the tiltmeters situated in the LDs, they detect rotations and/or bending of the YN1 endcap iron disks.

For the MAB structures the only monitored angle is Φ . Fig. 5 shows a sketch of a MAB with the position of the tiltmeter attached to it. The sensor is placed in an X–Y plane in order to detect a rotation of the structure around the Z axis. Small variations registered (μrads) with respect to the nominal Φ value of each particular MAB would indicate eventual tilts and/or deformations of the muon barrel wheels.

The data provided by the CMS Alignment System is handled by COCOA (CMS Object oriented Code for Optical Alignment [16]), an object oriented C++ software that allows the reconstruction, at any moment, of the CMS geometry. For the Muon alignment system, COCOA works with about 3000 parameters for the Link system, 6500 free parameters for the Endcap alignment system and for the Barrel alignment system with more than 20000 free parameters. In total, COCOA works with ~ 30000 degrees of freedom. The number of parameters together with the number of degrees of freedom measured by the system gives the level of redundancy with which the system is built.

The present study makes first a review of the CMS mechanical stability during the physics data taking periods along the six years of operation by investigating, as examples, a certain number of variables that were observed to be fully stable in Ref. [6].

Then, the research is focused on the distance between the LD and its corresponding AR, called $Z(\text{LD}–\text{AR})$, whose variation, $\Delta Z(\text{LD}–\text{AR})$, is monitored at three different Φ positions at both CMS Z sides ($\pm 75^\circ$, $\pm 195^\circ$ and $\pm 315^\circ$) by potentiometers located at the ARs in contact with targets mounted on $3609.691 \pm 0.033 \text{ mm}$ long Longitudinal Profiles (LPs) attached to the LDs [17,18]. The reason for this particular study is, as already mentioned, that these $\Delta Z(\text{LD}–\text{AR})$ distances were the only Link Alignment surveyed variables that, according to Ref. [7], do not present full stability 24 hours after the magnetic field reaches the working value (3.8 T as from 2009).

3. Magnet Cycles and Stability Periods.

A *Magnet Cycle* is defined as the operating time between the switching on and off of the current in the coils. The switch off is occasionally uncontrolled (*fast dump*): the current in the coils drops to 0 A in a few seconds. In these cases the magnet would take a minimum of a couple of days to restart working properly.

The lifetime of the CMS magnet is related to the number of magnet cycles. It is expected to be in the order of few hundred cycles. Tables 1 to 6 display the Magnet Cycles and the Stability Periods identified during the years 2008 to 2013, respectively. These tables indicate the cycle number, the starting date, the end of cycle date, the maximum magnetic field strength reached, the switch off conditions for that cycle, either through a slow ramp down (*controlled*) or through a fast ramp down (*fast dump*). Last two columns in the tables give a number to the Stability Period (if any) during the magnet cycle and the number of *stable days* completed.

Link alignment data are taken either each five minutes (usually during ramping up and down in field intensity, when the lasers are not in operation) or twice per day (during the periods at 3.8 or 4.0 T constant field, when the lasers are in use). Occasionally there is no data taken during a whole day in a cycle.

The CMS magnet field intensities as a function of the Link data number along the CMS 2008 - 2013 operations are shown on Fig. 6. In total there were 58 cycles, 30 of which finished with a fast dump. Only two cycles went up to $B = 4.0$ T (in November 2008). At the end of these two cycles, it was decided that the working magnetic field for physics runs would be 3.8 T. This field intensity is enough for high momentum charged particle bending and ensures a much better stability of the current in the coils (~ 18164 A) than that needed for 4 T (~ 19140 A).

The terms “link data number” or “event number” will be used throughout this document to designate the internal sequential data number during a given Link Alignment data taking, independently of whether the run corresponds to a given year, a magnet cycle or a stability period.

Physics data (cosmic rays, proton-proton or heavy ion collisions) are taken during the magnet periods at constant $B = 3.8$ T or 4 T (in the so-called *Stability Periods*). From 2008 to 2013 there were 42 of those stability periods, totalizing 771 days. Notice that not all the *Magnet Cycles* contain one or more *Stability Period*, as shown in Tables 1 to 6 for the years 2008 to 2013, respectively.

The ratio between the number of *stability days* and the number of *operation days* (days in which the coils receive current) in a given year may give an idea of the *efficiency of the operation* over that year. Table 7 displays this information for the period 2008 – 2013. As seen in column 4, the efficiency grows (but for the year 2011) with the expertise and the running of the LHC, from 10% in 2008 to 85% in 2013. In all, from a total of 1272 days of CMS underground operation, 771 were stable days during the data taking, that corresponds to an average CMS operating efficiency of 60.6%. The definition for efficiency used here it is not related to the ratio between the luminosity delivered by LHC and the one recorded by CMS. It is important to recall that a *Stability Period*, in the present study, starts 24 hours after the working magnetic field intensity is reached.

4. Results from the monitoring of the variables assumed to be mechanically stable: some examples

According to previous studies [6-7] it seems that, excluding the LD to AR relative distance, after the first 24 h at B_{\max} , CMS was *absolutely* stable, i.e. all possible motions, translations and tilts, stayed within the sensors' measurement resolutions: ~ 40 μm for displacements and ~ 40 μrad for rotations.

The present Section will be devoted to show that this was the case all along the 2008-2013 operating period by inspecting the behaviour of the recorded measurements corresponding to the following 48 variables (see Fig. 4):

- i) the relative axial distance between the Transfer Plates (TPs) and their nearest ME/1/1 Endcap Muon Chamber, $\Delta Z(\text{TP-ME11})$,
- ii) the relative radial distance between the external MABs and their nearest ME/1/2 Endcap Muon Chamber, $\Delta R(\text{MAB-ME12})$,
- iii) the relative radial distance between the TPs and their nearest ME/1/2, $\Delta R(\text{TP-ME12})$ and
- iv) the angular rotations of the Barrel Muon Chambers (see also Fig. 5).

Each observable is measured at the six Φ sectors (15, 75, 135, 195, 255 and 315 arc. deg. respectively) at both CMS Z sides.

The 42 Stability Periods listed in Tables 1 to 6 were analysed. In what follows we present, as examples, results from the following six sets of Operation Year–Stability Period (OY–SP) data, arbitrary chosen: 2008–SP1, 2009–SP4, 2010–SP1, 2011–SP2, 2012–SP2 and 2013–SP1.

4.1 The relative axial distance between the Transfer Plates and their nearest ME/1/1 Endcap Muon Chamber, $\Delta Z(\text{TP-ME11})$

The $Z(\text{TP-ME11})$ distance is measured by a contact Sakae potentiometer installed in the Transfer Plate touching a target located on the top side of the ME/1/1 Endcap Muon Chamber as sketched in Fig. 4.

The observed axial motion between the TP and the ME/1/1 when the field magnet goes from 0 to 3.8 T (in the years 2009 to 2013) indicates that TP moves apart from ME/1/1 an average value of $\langle Z \rangle = 1262.0 \pm 305.8$ μm at the CMS Z+ side, while for Z– the averaged displacement was $\langle Z \rangle = 1540.5 \pm 244.9$ μm . The quoted errors are only statistical (the RMS of the various measurements) and give an idea of how different can be the displacement from Magnet Cycle to Magnet Cycle and from sector to sector in Φ .

The relative $\Delta Z(\text{TP-ME11})$ distance is calculated as: $\Delta Z(\text{TP-ME11}) = Z(\text{TP-ME11})_{\text{data-number}} - Z(\text{TP-ME11})_{\text{initial}}$, where the $Z(\text{TP-ME11})_{\text{initial}}$ value corresponds to the first data taken, at each of the twelve Φ positions, 24 hours after B_{\max} is reached in each of the considered OY–SP data sets.

The evolution of the $\Delta Z(\text{TP-ME11})$ relative distance as a function of the Link Data Number is illustrated on Fig. 7, for various Φ sectors, while Table 8 displays, for all sectors in the six OY–SP data sets considered, the extreme value of the corresponding ΔZ distribution. The mention OO in the table means that the sensor was *out of order* during the corresponding data period.

A negative sign in the ΔZ value would correspond to an apparent mechanical approach of the TP to the ME/1/1, while a positive value would evidence that TP and ME/1/1 move apart. Motions appear to stay within the sensors measurement resolution.

4.2 The relative radial distance between the Transfer Plates and their nearest ME/1/2 Endcap Muon Chamber, $\Delta R(TP-ME12)$

The radial distance between the TP and the bottom side of its nearest ME/1/2 chamber, $R(TP-ME12)$, is also monitored using a contact potentiometer as sketched in Fig. 4.

The observed radial motion between the TP and the ME/1/2 Chamber, when the field magnet goes from 0 to 3.8 T (in the years 2009 to 2013) indicates that TP moves apart from ME12 an average value of $\langle R \rangle = 2764.4 \pm 236.5 \mu\text{m}$ at the CMS Z+ side, while for Z- the averaged displacement was $\langle R \rangle = 2883.5 \pm 246.3 \mu\text{m}$. The quoted errors are the RMS of the different measurements and evidence, also for this radial displacement, how different in amplitude can be the same motion under identical Magnetic Field strength variation.

The relative $\Delta R(TP-ME12)$ distance is calculated by $\Delta R(TP-ME12) = R(TP-ME12)_{\text{data-number}} - R(TP-ME12)_{\text{initial}}$ where the $R(TP-ME12)_{\text{initial}}$ value corresponds to the first data taken, at each of the twelve Φ positions, 24 hours after B_{max} is reached in each of the OY-SP considered.

How the $\Delta R(TP-ME12)$ value evolves as a function of the Link Data Number is illustrated in Fig. 8, for the same Φ sectors used in Fig.7 for the $\Delta Z(TP-ME11)$ motion. Table 9 displays the extreme values of the $\Delta R(TP-ME12)$ distributions for the six Φ sectors in the six OY-SP checked. Here one should also notice that a negative sign in the ΔR value would correspond to a TP to ME/1/2 apparent mechanical approach while a positive value would evidence that TP and ME/1/2 move apart. As seen, motions stay within the sensors measurement resolution.

4.3 The relative radial distance between the External MABs and their nearest ME/1/2 Endcap Muon Chamber, $\Delta R(MAB-ME12)$

The radial distance between the MAB and the outer side of the ME/1/2 chamber is monitored using a non-contact proximity sensor (Omron [13]) installed at the innermost part of each MAB structure. The sensor emitting/receiving head directs a laser light and receives the reflected light to/from a reflective target located on the outer region of the ME/1/2 chamber, as sketched in Fig. 4.

In this case, when the magnetic field increases from 0 to 3.8 T, the External MABs approach their corresponding ME/1/2 Chambers in a very small amount, $\langle R \rangle = -274.5 \pm 34.6 \mu\text{m}$ at the CMS Z+ side, while for Z- the measured averaged displacement was $\langle R \rangle = -262.8 \pm 31.8 \mu\text{m}$. The negative sign indicates that both structures approach each other, due probably to the observed deformation of the first end-cap disk.

For the relative displacements the used function was $\Delta R(MAB-ME12) = R(MAB-ME12)_{\text{data-number}} - R(MAB-ME12)_{\text{initial}}$ where the $R(MAB-ME12)_{\text{initial}}$ value corresponds to the first data taken, at each of the twelve Φ positions, 24 hours after B_{max} is reached in each of the OY-SP considered.

Fig. 9 illustrates, for some Φ sectors at positive and negative CMS Z sides during the considered OY–SP data taking periods, the recorded data as a function of the Link Data number. For this variable we have chosen Φ sectors showing the greatest measured motions.

The non-contact measuring sensors show that, in general, the MAB to ME12 relative distance increases, in a monotone way, with time (Link Data Number). In addition, a data-to-data 10 to 20 μm difference can be appreciated in some data collections. The origins of both phenomena remain unclear. In any case, the plotted ΔR values in Fig. 9, and the corresponding quoted values on Table 10 all remain within the measurement resolution for the used sensors ($\sim 40 \mu\text{m}$ as well), but one data in the 2010–SP1 at sector $\Phi = -255^\circ$ that exhibits a negligible deviation ($40.9 \mu\text{m}$).

4.4 Measurement of Barrel Muon Chamber rotations as detected with tiltmeter sensors at the External MABs

Eventual Barrel Muon Chambers rotations in Φ are monitored with AGI [14] tiltmeter sensors, whose position at the external MABs is sketched in Fig. 5. The sensors resolution is about 40 μrad . There are six External MABs at each Z end of the Barrel.

The sensor output is a voltage that is directly converted into an angle [15]. All the tiltmeters in the MABs are one dimensional sensors located in a X–Y plane, either at positive or negative values of the CMS Z coordinate. A positive increase in the output voltage translates into a $\Delta\Phi$ tilt or rotation in the direction of the positive Φ . A decrease in the output voltage means a $\Delta\Phi$ tilt in the direction of negative Φ . As will be shown, and apart from a couple of exceptions, the detected rotations during the Stability Periods will remain below the sensor resolution, therefore compatible with mechanical stability of the Barrel Muon Chambers. Nevertheless one should notice that when the current in the coil starts to increase and the field strength reaches B_{max} (4 T in 2008 and 3.8 T from 2009 on), the sensors at the external MABs (at both CMS Z sides) show clear start-up tilts that stop 24 h after B_{max} is reached.

Fig. 10 illustrates those motions for some of the Magnet Cycles (MC) containing the Stability Periods investigated in this document. The value of $\Delta\Phi$ is calculated with respect to the initial inclination of the sensor at $B = 0 \text{ T}$ and it is shown in the Figure as a function of the Link Data Number of the MC in question.

For the Stability periods, the $\Delta\Phi$ rotations are calculated as $\Delta\Phi(\text{MAB}) = \Delta\Phi(\text{MAB})_{\text{data-number}} - \Delta\Phi(\text{MAB})_{\text{initial}}$ where the $\Delta\Phi(\text{MAB})_{\text{initial}}$ value corresponds to the first data taken, at each of the twelve external MAB positions, 24 hours after B_{max} is reached in each of the OY–SP considered.

Fig. 11 illustrates, for some Φ sectors at positive and negative CMS Z sides during the considered OY–SP data taking periods, the calculated $\Delta\Phi(\text{MAB})$ relative to the AGI sensors recorded tilt as a function of the Link Data number. Table 11 displays the extreme values of the $\Delta\Phi(\text{MAB})$ distributions for the twelve Φ sectors in the six OY–SP used. All of them show values below the tiltmeters resolution.

5. Results of the measurements of the Z(LD-AR) distances during the Magnet Cycles along the 2008 – 2013 CMS operations.

The axial distance Z , between the LD and the AR in each of the CMS Z-sides is measured by means of a long aluminium profile (LP in Fig. 4) and a short distance measurement potentiometer. There are three LPs per Z-side. The LPs are attached to the corresponding LD and sustained in its middle length from the HE calorimeter.

A target installed at the end of the LP is touched by the rod of a Sakae potentiometer located in the AR. The quantity readout by the Link System is a resistance proportional to the rod position. When the LDs move towards their corresponding ARs by the action of the magnetic forces when passing from 0 T to B_{\max} , the targets on the LPs push the rods of the potentiometers. On the contrary, when the current in the coil goes down to zero the reading of the sensors indicate how much the LDs move apart from their corresponding ARs.

Fig. 12 shows, as an illustration, the 2011 operation. In the vertical scale the measured $Z(\text{LD-AR})$ distance is given, in mm, as a function of the Link Data Number, showing the motions at the six Φ angles (three per Z side). As seen from the figure the LDs approach the ARs by around 15 mm due to the magnetic field forces when B reaches B_{\max} . When back to $B = 0$ T the LDs separate from their corresponding ARs by a similar amount to recover the initial positions.

The monitored relative distance ΔZ , of LD to AR, is defined as $\Delta Z(\text{LD-AR}) = Z(\text{LD-AR})_{\text{data-number}} - Z(\text{LD-AR})_{\text{initial}}$, where the initial $Z(\text{LD-AR})$ value is the distance recorded at $B = 0$ T (at the six Φ positions), before ramping up to the desired B_{\max} (4 or 3.8 T). Fig. 13 shows, as an example, $\Delta Z(\text{LD-AR})$ at the $\Phi = 75^\circ$ quadrant in the CMS +Z side during the first magnet cycle in 2012 (see Table 5), where the top figure is the histogram of the 228 ΔZ data points, with a maximum approaching motion registered of 14.99 mm; the middle figure gives ΔZ as a function of the Link Data Number (at the last two data points, $B = 0$ T and LD returns around its initial position); and the bottom figure shows ΔZ as a function of the magnetic field intensity showing the expected quadratic behaviour [7].

The relative LD-AR distance, although quite similar between different magnet cycles, is far from being identical for all of them. To illustrate this point we show in Table 12, for the 3.8 T operations, the following quantities: the operation year, the number of 3.8 T Magnet Cycles during the given year (column 2), and the average of the maximum approach of the LD to its corresponding AR recorded at the six Φ positions (columns 3 to 8) over the cycles in column 2. Errors correspond to one standard deviation. It is clear that for the same magnetic field intensity the average maximum motions of LDs towards their corresponding ARs are different, well beyond one standard deviation, among the various years of observations. Note that the measured motion would also depend on the actual closing position of the first end-cap disk.

In addition to the fact that same magnetic field forces produce different motion amplitudes in the approaching of the LDs to their corresponding ARs, Table 12 also shows something systematic: the axial motions in the +Z CMS side are about 4.8 % larger than in the -Z side for all 6 monitored years, indicating probably a different return field and therefore a different magnetic force, possibly due to the different instrumentation of the forward region.

6. Study of the $\Delta Z(\text{LD-AR})$ measurements during the Stability Periods along the 2008 – 2013 CMS operations.

As shown in Tables 1 to 6, there were 42 Stability Periods at 3.8 T and 1 at 4.0 T along the years 2008 to 2013. As already said, the mechanical equilibrium that characterizes the SPs was questioned in Ref. [7] for the $\Delta Z(\text{LD-AR})$ relative distance: the magnitude most affected by the magnetic field forces. Therefore, the ΔZ distributions at the six Φ positions were studied in these 42 SPs. As before, the quantity ΔZ is defined as $\Delta Z(\text{LD-AR}) = Z(\text{LD-AR})_{\text{data-number}} - Z(\text{LD-AR})_{\text{initial}}$ where the initial $Z(\text{LD-AR})$ value corresponds to the first data taken 24 hours after B_{max} is reached, at each of the six Φ positions,

For all the 42 Stability Periods in the six monitored years of operation, Fig.14 summarizes the $\Delta Z(\text{LD-AR})$ relative distances monitored by the LP-Sakae potentiometer sets. At each SP the two extreme monitored values registered are plotted: the black dots represent the maximum LD-AR approach (negative values) and the open circles correspond to the maximum LD-AR separation in the apparent “accordion” motion. In most of the cases either the approach or the separation (or even both) exceed the 40 μm resolution of the short distance measurement devices.

Fig. 15 is an illustration of the monitored $\Delta Z(\text{LD-AR})$ during some SPs (arbitrary chosen) along the six investigated years, where the measured $\Delta Z(\text{LD-AR})$ value is plotted as a function of the Link Data Number. For the years 2008 and 2009 a measurement is recorded every five minutes. In all other cases there is a maximum of two data points per SP day. The distributions are far from being constant or smooth over time and motions surpassing $\pm 40 \mu\text{m}$ are clearly seen. In what follows we will use some of these six, Operation Year – Stability Period (OY-SP), data sets for further illustrations.

When the current in the coil remains stable, as is the case during the SPs, there should be no motion due to change in magnetic forces. Under these circumstances the motions seen in Figs. 14 and 15 should correspond either to unknown but real small mechanical instabilities of the muon endcap system or other effects as for instance eventual temperature changes.

The length of the LPs, that would allow such movements, measured at the Alignment Laboratory in the ISRs before mounting in CMS, was on average $L = 3609.691 \pm 0.033$ mm referred to a temperature of 20 $^{\circ}\text{C}$ [17, 18]. Being made of aluminium, a change in the temperature of the profile by an amount ΔT ($^{\circ}\text{C}$) = T_{measured} ($^{\circ}\text{C}$) – 20 ($^{\circ}\text{C}$) will result in a change of the length of the order of ΔL (μm) = 24 ($\mu\text{m m}^{-1} \text{ }^{\circ}\text{C}^{-1}$) \times 3.609691 (m) \times ΔT ($^{\circ}\text{C}$). In that case the relative $\Delta Z(\text{LD-AR})$ distance would be affected by eventual temperature changes, as shown in what follows.

6.1 Temperature monitoring in the LDs to ARs CMS air volumes.

PT100 temperature probes monitor the temperature in the neighbourhoods of the LPs. At the Link Disks there are probes at the six Φ sextants (15, 75, 135, 195, 255 and 315 arc. deg. respectively) at both +Z and -Z CMS sides. At the Alignment Rings there are two probes at $\Phi = 90$ and 270 arc. deg. respectively.

The temperature in the proximities of the Link Disks (TLD at + or - Z CMS side) associated to a recorded Link Data is defined as the average value of the six

corresponding PT100 probes. The one in the proximities of the Alignment Rings (TAR+ or TAR-) is taken as the average of the two corresponding PT100 probes. The temperature in the air volume between the Link Disks and the Alignment Rings associated to a recorded Link Alignment Data is calculated as the mean value of TLD and TAR at the considered Z side (represented by T+ and T- in what follows).

The calculated mean value of the temperature in the neighbourhoods of the aluminium profiles for the SPs recorded during the $\Delta Z(\text{LD}-\text{AR})$ monitoring in Fig. 15 are displayed in Fig. 16 as a function of the Link Data Number. The plotted mean temperature values correspond to the same CMS Z sides as the Φ angles in Fig. 15. Correlations between bumps in one figure and dips in the other (and vice versa) can be appreciated.

The numerical values of the monitored temperatures in the Link Disks – Alignment Rings volumes are given in Table 13 for the years and the Stability Periods used in the text and in Fig. 16 as examples. Columns 2 to 4 correspond to the Z+ CMS side. Column 2 gives the average temperature measured at the Link Disk (over six PT100 sensors); column 3 is the average (over two PT100 sensors) at the Alignment Ring. Column 4 (T+) gives the average value of the measurements taken at the Link Disk and the Alignment Ring that will be assumed to be the Longitudinal Profiles temperature. Columns 5 to 7 are the corresponding values measured at the Z- CMS side. All measurements are given in °C and the errors are the RMS of the corresponding distributions. A PT100 sensor has a resolution better than 0.01 °C.

Table 13 shows that the temperatures at the Alignment Rings (TAR, in both Z CMS sides) are much smaller (given the RMS values) than those at the Link Disks (TLD) neighborhoods most probably due to the Tracker operational conditions. A second observation is that the average temperature (T), in the LD-AR volume (the one to be assigned to the aluminum Longitudinal Profiles, LPs), is slightly higher (~1°C) at the CMS Z- side than at the Z+ side.

Among the six OY-SP sets appearing in Table 13 a detailed representation for the 2010-SP1 data, taken as example, is shown in Fig. 17, where the monitored temperature is plotted as a function of the Link Data Number. The left column of drawings in the figure corresponds to the CMS Z+ side. The three plots represent, respectively, the temperature measured near the Link Disk (TLD, averaged over 6 PT100 sensors), near the Alignment Ring (TAR, averaged over 2 PT100 sensors) and the assumed LP temperature, $T = (\text{TLD} + \text{TAR})/2$, in the air volume around the Long aluminum Profiles joining the Link Disk to its corresponding Alignment Ring. The three drawings of the right column correspond to the recorded data at the CMS Z- side. As seen in the figure, the temperature in the LD and AR neighborhoods and therefore in the volume around the LPs, changes almost continuously, following no smooth patterns.

The observation of the six mentioned data sets shows that, while in the sets 2008-SP1 and 2009-SP4 the changes are just of a few tenths of °C, in the 2010-SP1 (Fig. 12), 2011-SP2 and 2012-SP2 data sets one can appreciate changes of more than 1 °C, more than 2 °C for the set 2011-SP2, and almost 4 °C for the set SP2-2012.

The non-smooth behavior of the monitored temperatures shows trends that suggest the existence of some air flows (hot or cold) near the ARs, as from 2010, denoting a possible change in the Central Tracker temperature control system.

Since a change of ± 1 °C of the LPs implies a change of about ± 86.6 μm in its length (twice the resolution of the short distances measurement potentiometers) the studies of the temperature behaviour in the six OY–SP data sets brings to the conclusion that the computed $\Delta Z(\text{LD–AR})$, in the corresponding data sets, would be affected by a systematic error of the order of $(T_i - T_{\text{initial}}) \times 86.6$ $\mu\text{m}/^\circ\text{C}$, where T_i is the recorded temperature when computing the $Z(\text{LD–AR})$ distance at the Link Data Number “i” and T_{initial} the corresponding temperature for the first data in that particular SP. Therefore, correlations between the measured $\Delta Z(\text{LD–AR})$ and ΔT , if they exist, may explain the observed “accordion” motion.

6.2 Looking for $[\Delta Z(\text{LD–AR}) - T]$ and $[\Delta Z(\text{LD–AR}) - \Delta T]$ correlations.

A display of $\Delta Z(\text{LD–AR})$ in six different Φ sectors, versus the average temperature in the corresponding CMS Z side, at the time the measurement is done, is shown in Fig. 18. The data corresponds to six OY–SP data sets used as examples. The gaps do not correspond to missing data but they are due to changes in the temperature as the ones observed in Fig. 17.

Correlations between the monitored $\Delta Z(\text{LD–AR})$ and the average temperature T of the involved LP, are clearly observed. To illustrate this point Fig. 19 shows, for the 2010–SP1 data set, the following simultaneously monitored measurements: $\Delta Z(\text{LD–AR})$ as a function of the Link Data Number (top plot), the temperature T in the air volume around of the Long Aluminium Profiles joining the Link Disks to their corresponding Alignment Rings in the given CMS Z side ($TZ +$ or $-$) as a function of the Link Data Number (middle plot) and the $\Delta Z(\text{LD–AR})$ as a function of the reconstructed $\Delta T = (T_{\text{data-number}} - T_{\text{initial}})$ (bottom plot). The straight line over the data points corresponds to a linear fit to the data. The initial $Z(\text{LD–AR})$ and T values correspond to those of the first data taken, at the indicated (Φ , Z side) position, 24 hours after B_{max} is reached. The fitted function is of the type ΔZ (μm) = Constant ($\mu\text{m}^\circ\text{C}^{-1}$) \times ΔT ($^\circ\text{C}$) + Offset (μm).

The ΔZ – ΔT correlation is quite evident: when the temperature increases with respect to the first value in the SP, the length of the affected aluminium profile (LP) increases, the potentiometers get compressed, and therefore the LD–AR relative distance appears to decrease as if the LD approached the corresponding AR.

The above ΔZ – ΔT correlation is observed in all of the collected data along the six years of operation. For adding examples we give in Table 14 the results from the linear fits of the form ΔZ (μm) = Constant ($\mu\text{m}^\circ\text{C}^{-1}$) \times ΔT ($^\circ\text{C}$) + Offset (μm) done to the ΔZ – ΔT data sets appearing in column 1 for the Φ sectors appearing in column 2.

In all cases the offsets are omitted. The fitted constant has to be compared with the expected “theoretical” value of ± 86.6 $\mu\text{m}/^\circ\text{C}$. The sign is given by that of ΔT . The value of T_{initial} , main input for the fit, is also given.

These results explain the detected accordion motion: the Longitudinal Profiles stretch or shrink, according to the sign and the size of $\Delta T = (T_i - T_{\text{initial}})$, when recording the data number “i”. The core of CMS does not move during the Stability Periods; Link Disks and Alignment Rings do not move with respect to each other.

In consequence, it can be concluded that CMS was perfectly stable, also in this variable, during the data taking all along the first six years of operation.

7. Summary and conclusions

The present study of the Link alignment Data collected during the years 2008 to 2013 extends, with significantly more statistics, previous analysis on the motion and stability of the CMS structures.

The analysis [6, 7] of the Link Alignment data recorded during the CRAFT08 and the CRAFT09 runs suggested that the CMS detector stabilizes within the first 24 hours after the magnetic field reaches the nominal intensity of $B = 3.8$ T, given that displacements between mechanical structures beyond this time do not exceed the instrumental resolution of the monitoring sensors.

A later study performed in 2010 for seven different time periods over eight months to measure motions at constant $B = 3.8$ T magnetic field showed that the expected mechanical stability is not observed everywhere. In particular, the relative distance $\Delta Z(\text{LD}-\text{AR})$ in all of the six Φ sectors exhibits variations larger than the resolution of the sensors in most of the analyzed periods [7] thus questioning the idea of a *complete structural equilibrium*.

The present analysis, using data taken from the years 2008 to 2013, extends previous results and allows concluding that:

1. The study of the following 48 observables: i) the relative axial distance between the Transfer Plates (TPs) and their nearest ME/1/1 Endcap Muon Chamber, $\Delta Z(\text{TP}-\text{ME11})$, ii) the relative radial distance between the external MABs and their nearest ME/1/2 Endcap Muon Chamber, $\Delta R(\text{MAB}-\text{ME12})$, iii) the relative radial distance between the TPs and their nearest ME/1/2, $\Delta R(\text{TP}-\text{ME12})$ and iv) the angular rotations of the Barrel Muon Chambers, all presumed to remain stable during the Stability Periods, showed the expected absence of displacements, nor tilts, above the sensors measurement resolutions.
2. The study of the $\Delta Z(\text{LD}-\text{AR})-\Delta T$ correlation, observed in all of the collected data along the six years of operation, allows to determine that the so called out-of-stability variations detected on the $\Delta Z(\text{LD}-\text{AR})$ relative distance were not real, but a consequence of the systematic effects affecting the calculation of the monitored relative distances between the Link Disks and the Alignment Rings due to temperature changes during the physics data collection.

Altogether, this study summarizes the behavior of the CMS detector structures for the whole period from 2008 to 2013. The results lead to the conclusion that CMS was mechanically stable during the operation of the detector at constant magnetic field, which allowed excellent working conditions of the muon spectrometer and subsequent muon track reconstruction.

References

- [1] CMS Collaboration, “The CMS experiment at the CERN LHC”, JINST 3 (2008) S08004.
- [2] The CMS Collaboration, “The Magnet Project Technical Design Report”, CERN/LHCC 97-10.
- [3] The CMS Collaboration, “The Muon Project Technical Design Report”, CERN/LHCC 97-32.
- [4] The CMS Collaboration, “The Tracker Project Technical Design Report”, CERN/LHCC 98-06.
- [5] V. Karimaki and G. Wrochna, CMS TN/94-199; F. Matorras and A. Meneguzzo, CMS TN/95-069 and I. Belotelov et al. CMS NOTE 2006/017.
- [6] L.A. García Moral et al., Nucl. Instr. and Methods A 606 (2009) 344.
- [7] P. Arce et al., Nucl. Instr. And Methods A 675 (2012) 84.
- [8] M. Sobrón, “CMS detector geometry reconstructed with the Link alignment system”, PH. D. Thesis (2009), Instituto de Física de Cantabria, UC-CSIC, Santander, Spain.
- [9] A. Calderón et al., Nucl. Instr. and Methods A 565 (2006) 603.
- [10] A. Calderón et al., "Amorphous Silicon Position Detectors for the Link Alignment System of the CMS Detector: Users Handbook", Informe Técnico Ciemat 1126, December 2007.
- [11] C. Kholer et al., Nucl. Instr. and Methods A 608 (2009) 56.
- [12] Sakae Tsushin Kogyo Co., Ltd. - Trade Dept. 322 Ichinotsubo, Nakahara-ku, Kawasaki-city, Kanagawa-prefecture, 211-0016 Japan.
(<http://www.sakae-tsushin.co.jp>).
- [13] Omron Corporation, Tokyo Head Office, 3-4-10 Toranomom Minato-ku, Tokyo 105, Japan. (<http://www.omron.com>).
- [14] Applied Geomechanics Incorporated. 1336 Brommer Street, Santa Cruz, CA 95062 USA. (<http://www.geomechanics.com/>).
- [15] J. Alberdi et al., “Tiltmeters for the Alignment System of the CMS Experiment: Users Handbook”, Informe Técnico Ciemat 1107, May 2007.
- [16] P. Arce and A.L. Virto, “CMS Object Oriented Code for Optical Alignment (COCOA), CMS Note 2002/060, 2002.
- [17] J.F. Fuchs, R.Goudard and J.D. Mailefaud. “CMS-Alignment, Calibration of the 3 Longitudinal Profiles (Side +)”, January 2007, CMS-MA-UR-0076.
- [18] J.F. Fuchs, R.Goudard and J.D. Mailefaud. “CMS-Alignment, Calibration of the 3 Longitudinal Profiles (Side -)”, May 2007, CMS-MA-UR-0092.

Table Captions

Table 1: List of the Magnet Cycles (with their start and end dates) and of the Stability Periods (and how much they lasted) during the year 2008. The first data considered during a SP is the one taken 24 hours after the working magnetic field intensity is reached. In cycle number 1 the maximum magnetic field reached was only 2.1 T, whereas in cycles 12 and 13, 4.0 T was reached. No new attempt to reach that high field intensity was tried.

Table 2: List of the Magnet Cycles (with their start and end dates) and of the Stability Periods (and how much they lasted) during the year 2009. The first data considered during a SP is the one taken 24 hours after the working magnetic field intensity is reached. In cycles numbers 1 to 5 the 3.8 T intensity is not reached. In cycle number 14 there were five 3.8 T independent SPs, totalizing 19 days, before the current were switched off.

Table 3: List of the Magnet Cycles (with their start and end dates) and of the Stability Periods (and how much they lasted) during the year 2010. The first data considered during a SP is the one taken 24 hours after the working magnetic field intensity is reached. In cycle number 1 the 3.8 T field is not reached. During Magnet Cycle 13 there were five 3.8 T periods before the current went off in a non-controlled way.

Table 4: List of the Magnet Cycles (with their start and end dates) and of the Stability Periods (and how much they lasted) during the year 2011. The first data considered during a SP is the one taken 24 hours after the working magnetic field intensity is reached. Notice that in cycle number 1 the 3.8 T field is not reached. In addition, during cycle number 5 there was no time (the field was on for less than 24 hours) for any stability period at 3.8 T.

Table 5: List of the Magnet Cycles (with their start and end dates) and of the Stability Periods (and how much they lasted) during the year 2012. The first data considered during a SP is the one taken 24 hours after the working magnetic field intensity is reached. In cycle number 2 there were two 3.8 T stability periods (numbers 2 and 3 with 61 and 38 days duration, respectively) before the current were switched off.

Table 6: List of the Magnet Cycles (with their start and end dates) and of the Stability Periods (and how much they lasted) during the year 2013. The first data considered during a SP is the one taken 24 hours after the working magnetic field intensity is reached.

Table 7: Efficiency, defined as the ratio, in percentage, between the number of *stability days* and the number of *operation days*, of the physics data taking procedure per year and for the whole 2008 to 2013 CMS activity.

Table 8: For the years and Stability Periods used in the text as examples, indicated by OY/SP in Column 1, the extreme value of the $\Delta Z(\text{TP-ME11})$ distribution is given, in μm , for the analyzed $\pm\Phi$ sector. The sign in front of the Φ value indicates the CMS Z side. The angle Φ is given in arc. deg. A negative sign in the ΔZ value would correspond to a TP to ME/1/1 mechanical approach while a positive value would evidence that TP and ME/1/1 move apart. However, these apparent motions may also be a manifestation of small temperature changes in the area.

Table 9: For the years and Stability Periods used in the text as examples, indicated by OY/SP in Column 1, the extreme value of the $\Delta R(\text{TP-ME12})$ distribution is given, in μm , for the analyzed $\pm\Phi$ sector. The sign in front of the Φ value indicates the CMS Z

side. The angle Φ is given in arc. deg. A negative sign in the ΔR value would correspond to a TP to ME/1/2 mechanical approach while a positive value would evidence that TP and ME/1/2 move apart. However, these apparent motions may also be a manifestation of small temperature changes in the area.

Table 10: For the years and Stability Periods used in the text as examples, indicated by OY/SP in Column 1, the extreme value of the $\Delta R(\text{MAB}-\text{ME}12)$ distribution is given, in μm , for the analyzed $\pm\Phi$ sector. The sign in front of the Φ value indicates the CMS Z side. The angle Φ is given in arc. deg. A negative sign in the ΔR value would correspond to a MAB to ME/1/2 mechanical approach while a positive value would evidence that MAB and ME/1/2 move apart. Detected motions are most probably due to instabilities of the Omron sensors.

Table 11: For the years and Stability Periods used in the text as examples, indicated by OY/SP in Column 1, the extreme value of the $\Delta\Phi(\text{MAB})$ distribution is given, in μrad , for the analyzed $\pm\Phi$ External MAB as a function of the Link Data Number. Data are readout from AGI Tiltmeters with $\sim 40 \mu\text{rad}$ resolution.

Table 12: For the operations at 3.8 T. Column 1: Operation Year; column 2: number of cycles at $B_{\text{max}} = 3.8\text{T}$; columns 3 to 8: average ΔZ (LD-AR) values at the given Φ quarter (the sign corresponds to the CMS Z side). All measurements are given in mm. The errors are the standard deviation of the average. When there is only one cycle, the quoted error is the sensor resolution. The potentiometer at $\Phi = -75^\circ$ was out of order in the year 2008. Also the one at $\Phi = +195^\circ$ during the 2013 operation.

Table 13: For the Operation Year – Stability Period data set given in column 1, column 2 gives the average temperature measured at the Link Disk with six PT100 sensors, column 3 is the average (over two PT100 sensors) at the Alignment Rings and column 4 (T+) gives the average value of the measurements taken at the Link Disk and the Alignment Ring, representing the Longitudinal Profiles temperature. Columns 5 to 7 are the corresponding values measured at the Z– CMS side. All measurements are given in $^\circ\text{C}$. The errors are the RMS of the corresponding distribution. A PT100 sensor has a resolution better than $0.01 \text{ }^\circ\text{C}$.

Table 14: For the years and Stability Periods used in the text as examples and appearing in Column 1, and for the Zside/ Φ angle given in Column 2, results of the fitted C constants (Column 3) in the function $\Delta Z (\mu\text{m}) = C (\mu\text{m}/^\circ\text{C}) \times \Delta T (^\circ\text{C}) + O (\mu\text{m})$, with $\Delta T = (T_i - T_{\text{initial}})$, to be compared with the theoretical value $C_{\text{expected}} = 86.6 (\mu\text{m}/^\circ\text{C})$. Column 4 gives the χ^2/NDF of the corresponding fits. The input T_{initial} ($^\circ\text{C}$) value is given in Column 5. The offset (O) fitted value is considered irrelevant for the discussion.

Cycle nb.	Start date	End date	B_{\max} (T)	Switch off cond.	SP nb.	SP days
1	27/8	29/8	2.1	Controlled	None	0
2	29/8	8/9	3.0	Controlled	None	0
3	8/9	9/9	3.0	Controlled	None	0
4	7/10	10/10	3.8	Fast Dump	None	0
5	10/10	21/10	3.8	Controlled	1	4
6	21/10	21/10	3.8	Controlled	None	0
7	21/10	24/10	3.8	Controlled	None	0
8	24/10	6/11	3.8	Fast Dump	2	2
9	6/11	8/11	3.8	Controlled	3	2
10	8/11	12/11	3.8	Controlled	None	0
11	12/11	13/11	3.8	Fast Dump	None	0
12	13/11	14/11	4.0	Fast Dump	None	0
13	14/11	21/11	4.0	Fast Dump	4	1

Table 1: List of the Magnet Cycles (with their start and end dates) and of the Stability Periods (and how much they lasted) during the year 2008. The first data considered during a SP is the one taken 24 hours after the working magnetic field intensity is reached. In cycle number 1 the maximum magnetic field reached was only 2.1 T, whereas in cycles 12 and 13, 4.0 T was reached. No new attempt to reach that high field intensity was tried.

Cycle nb.	Start date	End date	B_{\max} (T)	Switch off cond.	SP nb.	SP days
1	17/6	9/7	1.0	Controlled	None	0
2	10/7	15/7	1.5	Controlled	None	0
3	16/7	24/7	2.0	Controlled	None	0
4	24/7	24/7	2.0	Fast Dump	None	0
5	27/7	28/7	2.0	Controlled	None	0
6	28/7	29/7	3.8	Fast Dump	1	1
7	7/8	11/8	3.8	Controlled	2	1
8	11/8	18/8	3.8	Controlled	3	7
9	18/8	18/8	3.8	Fast Dump	None	0
10	18/8	30/8	3.8	Controlled	4	5
11	31/8	31/8	3.8	Fast Dump	None	0
12	31/8	23/10	3.8	Fast Dump	None	0
13	26/10	17/11	3.8	Fast Dump	5	9
14	18/11	16/12	3.8	Controlled	6 - 10	19

Table 2: List of the Magnet Cycles (with their start and end dates) and of the Stability Periods (and how much they lasted) during the year 2009. The first data considered during a SP is the one taken 24 hours after the working magnetic field intensity is reached. In cycles numbers 1 to 5 the 3.8 T intensity is not reached. In cycle number 14 there were five 3.8 T independent SPs, totalizing 19 days, before the current were switched off.

Cycle nb.	Start date	End date	B _{max} (T)	Switch off cond.	SP nb.	SP days
1	21/1	10/2	1.	Controlled	None	0
2	10/2	15/2	3.8	Controlled	None	0
3	15/2	25/2	3.8	Controlled	None	0
4	25/2	15/4	3.8	Fast Dump	1	37
5	15/4	26/4	3.8	Fast Dump	2	8
6	26/4	31/5	3.8	Fast Dump	3	29
7	31/5	19/7	3.8	Controlled	4	45
8	19/7	3/8	3.8	Controlled	5	9
9	3/8	16/8	3.8	Controlled	6	13
10	16/8	30/8	3.8	Controlled	7	14
11	30/8	2/9	3.8	Fast Dump	None	0
12	2/9	19/10	3.8	Controlled	8	47
13	19/10	8/12	3.8	Fast Dump	9 - 13	40

Table 3: List of the Magnet Cycles (with their start and end dates) and of the Stability Periods (and how much they lasted) during the year 2010. The first data considered during a SP is the one taken 24 hours after the working magnetic field intensity is reached. In cycle number 1 the 3.8 T field is not reached. During Magnet Cycle 13 there were five 3.8 T periods before the current went off in a non-controlled way.

Cycle nb.	Start date	End date	B _{max} (T)	Switch off cond.	SP nb.	SP days
1	25/1	9/2	1.0	Controlled	None	0
2	9/2	28/3	3.8	Controlled	1	46
3	30/3	9/5	3.8	Fast Dump	2	24
4	10/5	29/6	3.8	Controlled	3	47
5	29/6	13/7	3.8	Controlled	None	0
6	14/7	6/10	3.8	Controlled	4	21
7	6/10	10/11	3.8	Controlled	5	25
8	1/11	8/11	3.8	Fast Dump	None	0
9	9/11	8/12	3.8	Controlled	6	26

Table 4: List of the Magnet Cycles (with their start and end dates) and of the Stability Periods (and how much they lasted) during the year 2011. The first data considered during a SP is the one taken 24 hours after the working magnetic field intensity is reached. Notice that in cycle number 1 the 3.8 T field is not reached. In addition, during cycle number 5 there was no time (the field was on for less than 24 hours) for any stability period at 3.8 T.

Cycle nb.	Start date	End date	B _{max} (T)	Switch off cond.	SP nb.	SP days
1	31/1	9/3	3.8	Fast Dump	1	2
2	9/3	20/6	3.8	Fast Dump	2 - 3	99
3	20/6	10/8	3.8	Fast Dump	4	41
4	11/8	22/8	3.8	Fast Dump	5	6
5	22/8	17/9	3.8	Controlled	6	33
6	17/9	17/9	3.8	Fast Dump	None	0
7	20/9	26/11	3.8	Controlled	7	64
8	26/11	18/12	3.8	Fast Dump	8	18

Table 5: List of the Magnet Cycles (with their start and end dates) and of the Stability Periods (and how much they lasted) during the year 2012. The first data considered during a SP is the one taken 24 hours after the working magnetic field intensity is reached. In cycle number 2 there were two 3.8 T stability periods (numbers 2 and 3 with 61 and 38 days duration, respectively) before the current were switched off.

Cycle nb.	Start date	End date	B_{\max} (T)	Switch off cond.	SP nb.	SP days
1	9/1	17/2	3.8	Fast Dump	1	34

Table 6: List of the Magnet Cycles (with their start and end dates) and of the Stability Periods (and how much they lasted) during the year 2013. The first data considered during a SP is the one taken 24 hours after the working magnetic field intensity is reached.

Year	Days of operation	Stability Days	Efficiency (%)
2008	87	9	10.3
2009	183	34	18.6
2010	322	242	75.2
2011	318	189	59.4
2012	322	263	81.7
2013	40	34	85.0
Total	1272	771	60.6

Table 7: Efficiency, defined as the ratio, in percentage, between the number of *stability days* and the number of *operation days*, of the physics data taking procedure per year and for the whole 2008 to 2013 CMS activity.

OY/SP	$\pm\Phi/\Delta Z$					
2008/SP1	+15/10.0	+75/12.4	+135/20.0	+195/00	+255/00	+315/6.8
	-15/10.0	-75/-15.1	-135/14.1	-195/-10.7	-255/10.0	-315/12.7
2009/SP4	+15/-12.3	+75/-15.1	+135/-15.0	+195/-15.0	+255/-39.7	+315/-11.4
	-15/-17.1	-75/-23.2	-135/-30.5	-195/-16.2	-255/-12.0	-315/-10.7
2010/SP1	+15/10.6	+75/18.0	+135/24.6	+195/16.1	+255/00	+315/12.0
	-15/-16.1	-75/-30.2	-135/-23.6	-195/21.0	-255/16.7	-315/15.7
2011/SP2	+15/23.8	+75/27.8	+135/20.8	+195/18.7	+255/00	+315/15.0
	-15/21.9	-75/37.9	-135/26.8	-195/15.0	-255/14.8	-315/25.1
2012/SP2	+15/27.0	+75/35.0	+135/35.2	+195/24.3	+255/00	+315/26.5
	-15/37.7	-75/00	-135/00	-195/27.8	-255/35.8	-315/38.9
2013/SP1	+15/21.5	+75/38.3	+135/30.0	+195/6.5	+255/00	+315/22.3
	-15/27.4	-75/31.6	-135/33.3	-195/31.6	-255/33.3	-315/23.3

Table 8: For the years and Stability Periods used in the text as examples, indicated by OY/SP in Column 1, the extreme value of the $\Delta Z(\text{TP-ME11})$ distribution is given, in μm , for the analyzed $\pm\Phi$ sector. The sign in front of the Φ value indicates the CMS Z side. The angle Φ is given in arc. deg. A negative sign in the ΔZ value would correspond to a TP to ME/1/1 mechanical approach while a positive value would evidence that TP and ME/1/1 move apart. However, these apparent motions may also be a manifestation of small temperature changes in the area.

OY/SP	$\pm\Phi/\Delta R$					
2008/SP1	+15/-10.5	+75/-11.5	+135/-7.9	+195/00	+255/-15.3	+315/-10.0
	-15/-9.7	-75/-10.0	-135/-7.8	-195/20.0	-255/-12.0	-315/-11.1
2009/SP4	+15/-4.6	+75/-9.1	+135/12.8	+195/-7.7	+255/-6.0	+315/6.4
	-15/8.8	-75/-14.3	-135/-10.1	-195/-8.0	-255/-25.3	-315/-6.6
2010/SP1	+15/20.8	+75/22.9	+135/-13.1	+195/11.9	+255/11.8	+315/11.6
	-15/23.8	-75/-11.0	-135/-14.2	-195/-5.8	-255/29.8	-315/16.1
2011/SP2	+15/34.7	+75/35.2	+135/33.5	+195/22.5	+255/29.6	+315/31.7
	-15/21.5	-75/39.8	-135/34.4	-195/33.5	-255/00	-315/33.2
2012/SP2	+15/7.0	+75/7.6	+135/24.9	+195/11.6	+255/14.4	+315/7.9
	-15/14.7	-75/20.8	-135/18.4	-195/15.4	-255/27.8	-315/10.2
2013/SP1	+15/6.5	+75/25.5	+135/21.6	+195/5.5	+255/13.6	+315/6.3
	-15/17.6	-75/21.5	-135/24.0	-195/3.9	-255/25.5	-315/16.8

Table 9: For the years and Stability Periods used in the text as examples, indicated by OY/SP in Column 1, the extreme value of the ΔR (TP–ME12) distribution is given, in μm , for the analyzed $\pm\Phi$ sector. The sign in front of the Φ value indicates the CMS Z side. The angle Φ is given in arc. deg. A negative sign in the ΔR value would correspond to a TP to ME/1/2 mechanical approach while a positive value would evidence that TP and ME/1/2 move apart. However, these apparent motions may also be a manifestation of small temperature changes in the area.

OY/SP	$\pm\Phi/\Delta R$					
2008/SP1	+15/1.8	+75/00	+135/11.8	+195/15.0	+255/13.7	+315/-5.1
	-15/00	-75/00	-135/20.0	-195/10.9	-255/20.0	-315/00
2009/SP4	+15/-2.3	+75/00	+135/13.2	+195/-13.2	+255/14.3	+315/2.1
	-15/00	-75/00	-135/00	-195/-10.3	-255/15.1	-315/-4.7
2010/SP1	+15/7.1	+75/8.2	+135/-13.1	+195/-14.2	+255/-12.4	+315/4.9
	-15/10.0	-75/00	-135/00	-195/20.0	-255/40.9	-315/10.9
2011/SP2	+15/00	+75/6.8	+135/-13.1	+195/-15.3	+255/-15.4	+315/6.8
	-15/10.1	-75/00	-135/00	-195/10.9	-255/37.4	-315/00
2012/SP2	+15/00	+75/20.5	+135/33.2	+195/33.2	+255/36.7	+315/00
	-15/4.9	-75/00	-135/00	-195/24.9	-255/00	-315/00
2013/SP1	+15/00	+75/15.9	+135/-8.5	+195/14.3	+255/15.3	+315/-4.6
	-15/5.4	-75/00	-135/00	-195/9.4	-255/00	-315/00

Table 10: For the years and Stability Periods used in the text as examples, indicated by OY/SP in Column 1, the extreme value of the $\Delta R(\text{MAB}-\text{ME}12)$ distribution is given, in μm , for the analyzed $\pm\Phi$ sector. The sign in front of the Φ value indicates the CMS Z side. The angle Φ is given in arc. deg. A negative sign in the ΔR value would correspond to a MAB to ME/1/2 mechanical approach while a positive value would evidence that MAB and ME/1/2 move apart. Detected motions are most probably due to instabilities of the Omron sensors.

OY/SP	$\pm\Phi$ sect./ max. $\Delta\Phi$					
2008/SP1	+15/-1.2	+75/2.7	+135/-11.2	+195/7.9	+255/-7.1	+315/12.4
	-15/15.9	-75/8.6	-135/OO	-195/OO	-255/20.0	-315/-16.7
2009/SP4	+15/-4.2	+75/2.3	+135/-15.3	+195/-3.2	+255/5.1	+315/2.7
	-15/2.8	-75/-4.7	-135/OO	-195/OO	-255/12.8	-315/-5.1
2010/SP1	+15/1.5	+75/-2.2	+135/-3.0	+195/-3.3	+255/-2.3	+315/2.3
	-15/4.5	-75/2.7	-135/OO	-195/OO	-255/-2.3	-315/-4.1
2011/SP2	+15/-5.0	+75/-3.1	+135/3.6	+195/-5.6	+255/6.5	+315/-5.8
	-15/4.7	-75/4.7	-135/-37.3	-195/OO	-255/-9.2	-315/OO
2012/SP2	+15/1.8	+75/-2.2	+135/-2.8	+195/2.8	+255/-5.0	+315/-31.1
	-15/7.9	-75/3.9	-135/-19.1	-195/-2.2	-255/2.3	-315/OO
2013/SP1	+15/3.4	+75/3.9	+135/-4.9	+195/4.9	+255/4.3	+315/5.8
	-15/-5.8	-75/-3.9	-135/-6.5	-195/-4.3	-255/-6.2	-315/OO

Table 11: For the years and Stability Periods used in the text as examples, indicated by OY/SP in Column 1, the extreme value of the $\Delta\Phi$ (MAB) distribution is given, in μrad , for the analyzed $\pm\Phi$ External MAB as a function of the Link Data Number. Data are readout from AGI Tiltmeters with $\sim 40 \mu\text{rad}$ resolution.

Year	#Cycles	+75°	+195°	+315°	-75°	-195°	-315°
2008	8	14.85±0.11	15.15±0.11	15.25±0.23	---	13.52±0.15	14.34±0.20
2009	8	14.28±0.10	14.58±0.10	14.60±0.15	13.90±0.18	13.35±0.05	14.03±0.14
2010	12	14.25±0.12	14.50±0.12	14.55±0.15	13.96±0.14	13.57±0.09	14.26±0.09
2011	8	14.25±0.10	14.53±0.11	14.54±0.11	13.73±0.09	13.34±0.03	13.77±0.16
2012	8	13.85±0.14	14.02±0.24	14.12±0.14	13.68±0.07	13.47±0.13	13.71±0.12
2013	1	11.30±0.04	---	14.23±0.04	13.66±0.04	13.66±0.04	13.95±0.04

Table 12: For the operations at 3.8 T. Column 1: Operation Year; column 2: number of cycles at $B_{\max} = 3.8T$; columns 3 to 8: average ΔZ (LD-AR) values at the given Φ quarter (the sign corresponds to the CMS Z side). All measurements are given in mm. The errors are the standard deviation of the average. When there is only one cycle, the quoted error is the sensor resolution. The potentiometer at $\Phi = -75^\circ$ was out of order in the year 2008. Also the one at $\Phi = +195^\circ$ during the 2013 operation.

OY-SP	TLD +	TAR +	T +	TLD -	TAR -	T -
2008-SP1	21.69±0.16	19.85±0.06	20.77±0.11	21.62±0.13	20.46±0.04	21.04±0.08
2009-SP4	20.10±0.13	16.58±0.06	18.34±0.05	20.20±0.12	17.74±0.05	18.97±0.04
2010-SP1	20.76±0.05	15.33±1.25	18.04±0.63	20.81±0.04	18.25±1.16	19.53±0.59
2011-SP2	19.35±0.06	14.98±1.49	17.17±0.76	19.43±0.06	16.09±1.28	17.76±0.66
2012-SP2	19.22±0.14	11.55±1.97	15.38±1.00	19.21±0.13	12.91±1.78	16.06±0.90
2013-SP1	19.20±0.30	11.10±0.50	15.20±0.30	19.30±0.40	12.50±0.50	15.90±0.30

Table 13: For the Operation Year – Stability Period data set given in column 1, column 2 gives the average temperature measured at the Link Disk with six PT100 sensors, column 3 is the average (over two PT100 sensors) at the Alignment Rings and column 4 (T+) gives the average value of the measurements taken at the Link Disk and the Alignment Ring, representing the Longitudinal Profiles temperature. Columns 5 to 7 are the corresponding values measured at the Z- CMS side. All measurements are given in °C. The errors are the RMS of the corresponding distribution. A PT100 sensor has a resolution better than 0.01 °C.

OY–SP	(Zside) Φ (arc. deg.)	C_{fitted} ($\mu\text{m}/^{\circ}\text{C}$)	χ^2/NDF	T_{initial} ($^{\circ}\text{C}$)
2008–SP1	+ 75	-360.7 ± 20.0	20/359	20.64
2008–SP1	+ 195	-253.7 ± 20.0	11/359	20.64
2009–SP4	– 195	-129.2 ± 23.3	68/1309	17.88
2009–SP4	+ 195	-25.6 ± 21.7	23/1309	18.27
2010–SP1	+ 315	-71.6 ± 9.5	50/42	17.24
2010–SP1	+ 195	-73.7 ± 9.5	53/42	17.24
2011–SP2	– 75	-43.2 ± 9.4	5/40	17.80
2011–SP2	+ 195	-18.7 ± 8.1	40/40	17.23
2012–SP2	– 315	-43.1 ± 4.5	59/96	16.00
2012–SP2	+ 195	-46.3 ± 4.1	157/96	15.03
2013–SP1	– 75	-55.8 ± 19.3	4/62	15.78
2013–SP1	+ 195	-24.6 ± 17.1	11/62	14.91

Table 14: For the years and Stability Periods used in the text as examples and appearing in Column 1, and for the Zside/ Φ angle given in Column 2, results of the fitted C constants (Column 3) in the function ΔZ (μm) = C ($\mu\text{m}/^{\circ}\text{C}$) \times ΔT ($^{\circ}\text{C}$) + O (μm), with $\Delta T = (T_i - T_{\text{initial}})$, to be compared with the theoretical value $C_{\text{expected}} = 86.6$ ($\mu\text{m}/^{\circ}\text{C}$). Column 4 gives the χ^2/NDF of the corresponding fits. The input T_{initial} ($^{\circ}\text{C}$) value is given in Column 5. The offset (O) fitted value is considered irrelevant for the discussion.

Figure captions

Fig. 1: Longitudinal view of one quadrant of the CMS detector. The positions of the Z-stops are indicated. Laser lines (in dashed) used for the Alignment System are also shown, except for the barrel region.

Fig. 2: Sketch of the deformation of the endcap iron disks as a result of the compression due to the magnetic field forces and the resistance of the barrel Z-stops.

Fig. 3: Schematic view of the Alignment System. a): one Φ alignment plane. The continuous and dotted lines show different optical paths. b): transverse view of the barrel muon detectors. The crossing lines indicate the three alignment Φ planes. The CMS coordinate system is also indicated in the figure.

Fig. 4: Sketch of main Link Alignment elements (not to scale) in a quadrant of a Φ plane. The distances whose variations were used to study the evolution of deformations are $R(\text{MAB-ME1/2})$, $Z(\text{TP-ME1/1})$ and $Z(\text{LD-AR})$. Tiltmeters and temperature sensors are not shown.

Fig. 5: A MAB structure, showing the position of the tiltmeter for Φ monitoring.

Fig. 6: The CMS magnetic field intensities as a function of the Link data number along the CMS 2008 - 2013 operations.

Fig 7: Evolution of the $\Delta Z(\text{TP-ME11})$ relative distance (vertical axis, in μm) as a function of the Link Data Number proper to the considered OP-SP data set, for different Φ sectors.

Fig. 8: Evolution the $\Delta R(\text{TP-ME12})$ value (vertical axis, in μm) as a function of the Link Data Number proper to the considered data set for the same Φ sectors used to illustrate the $\Delta Z(\text{TP-ME11})$ motion on Fig. 19.

Fig. 9: Relative $\Delta R(\text{MAB-ME12})$ radial distance (vertical axis, in μm) as a function of the Link Data number for some Φ sectors at positive and negative CMS Z sides during the considered OY-SP data taking periods. For this illustration we have chosen sectors showing the greatest measured motions.

Fig 10: Monitored $\Delta\Phi$ motions (vertical axis, in μrad) for some of the Magnet Cycles (MC) containing the Stability Periods investigated in this document. $\Delta\Phi$ is calculated with respect to the initial inclination of the sensor at $B = 0$ T and it is shown as a function of the Link Data Number of the MC in question.

Fig. 11: The reconstructed $\Delta\Phi(\text{MAB})$ rotations (vertical axis, in μrad) as a function of the Link Data number for some Φ sectors at positive and negative CMS Z sides during the considered OY-SP data taking periods. The sensors measuring the eventual tilts have a measured resolution of ~ 40 μrad .

Fig. 12: In the vertical axis, the Z (LD-AR) distance during the year 2011, monitored by the Sakae potentiometers at six Φ quadrants ($\pm 75^\circ$, $\pm 195^\circ$ and $\pm 315^\circ$, the sign refers to the CMS Z side) as a function of the link data number. There were 9 magnet cycles (see Table 4).

Fig. 13: ΔZ (LD-AR) monitored by the Sakae potentiometer at the $\Phi = +75^\circ$ quadrant, the sign refers to the CMS Z, during the first magnet cycle in 2012 (see Table 5). Top: histogram of data points. The maximum motion registered is -14.99 mm. Middle: ΔZ as a function of the Link Data Number. By the last data $B = 0$ T and LD returns to its

initial position. Bottom: ΔZ as a function of the magnetic field intensity showing the expected quadratic behaviour.

Fig. 14: $\Delta Z(\text{LD-AR})$ monitored by the Sakae potentiometers during the 42 Stability Periods along the 2008 to 2013 CMS years of operation. $\Delta Z(\text{LD-AR}) = Z(\text{LD-AR})_{\text{data-number}} - Z(\text{LD-AR})_{\text{initial}}$, where the initial $Z(\text{LD-AR})$ values are read out at $B = B_{\text{max}}$ (3.8 or 4 T) at the six Φ positions corresponding to the first data taken 24 hours after B_{max} is reached. For each SP the two extreme monitored values registered are shown: the black dots represent the maximum LD-AR approach (negative values) and the open circles correspond to the maximum LD-AR separation in the apparent “accordion” motion.

Fig. 15: $\Delta Z(\text{LD-AR})$ distance measurements, in microns, for the indicated Φ quadrant (sign refers to + or – Z CMS side) as a function of the Link Data Number during the indicated OY–SP.

Fig. 16: Averaged temperature, in °C, in the neighbourhoods of the aluminium profiles for the indicated CMS Z side (sign refers to the side) as a function of the Link Data Number during the mentioned OperationYear–StabilityPeriod data set. There is a one to one correspondence with the Φ quadrants in Fig. 10.

Fig. 17: Monitoring of the temperature during the SP1 in year 2010 as a function of the Link Data Number. Data are recorded twice per day. Most of the points represent two measurements superimposed. Left column corresponds to CMS Z+ side, the three plots represent the temperature measured near the Link Disk (6 PT100 sensors), the Alignment Ring (2 PT100 sensors) and the assumed temperature, $T = (\text{TLD} + \text{TAR})/2$, in the air volume around the Long Profiles joining the Link Disk to its corresponding Alignment Ring. Right column are the recorded data at the Z– side.

Fig 18: $\Delta Z(\text{LD-AR})$ distance measurements, in microns, for the indicated Φ quadrant (sign refers to + or – Z CMS side) versus the average temperature T , in °C, for the indicated CMS Z side (sign refers to the side), during the indicated Stability Period for the mentioned year. Although the correlations exist, their parametrization do not appear to be simple and unique.

Fig 19: Correlation of the measured $\Delta Z(\text{LD-AR})$ with the changes in the temperature in the air volume around the Longitudinal Profiles. In the case of this example the relation between the two measured quantities, with respect to those of the first data taking during the SP1 in the year 2010 at $\Phi = +315$, is $\Delta Z (\mu\text{m}) = (-71.6 \pm 9.5) (\mu\text{m}/^\circ\text{C}) \times \Delta T$ (°C), with $\chi^2/\text{NDF} = 50/42$. $\Delta T = T_{\text{data}} (\text{°C}) - 17.24 (\text{°C})$.

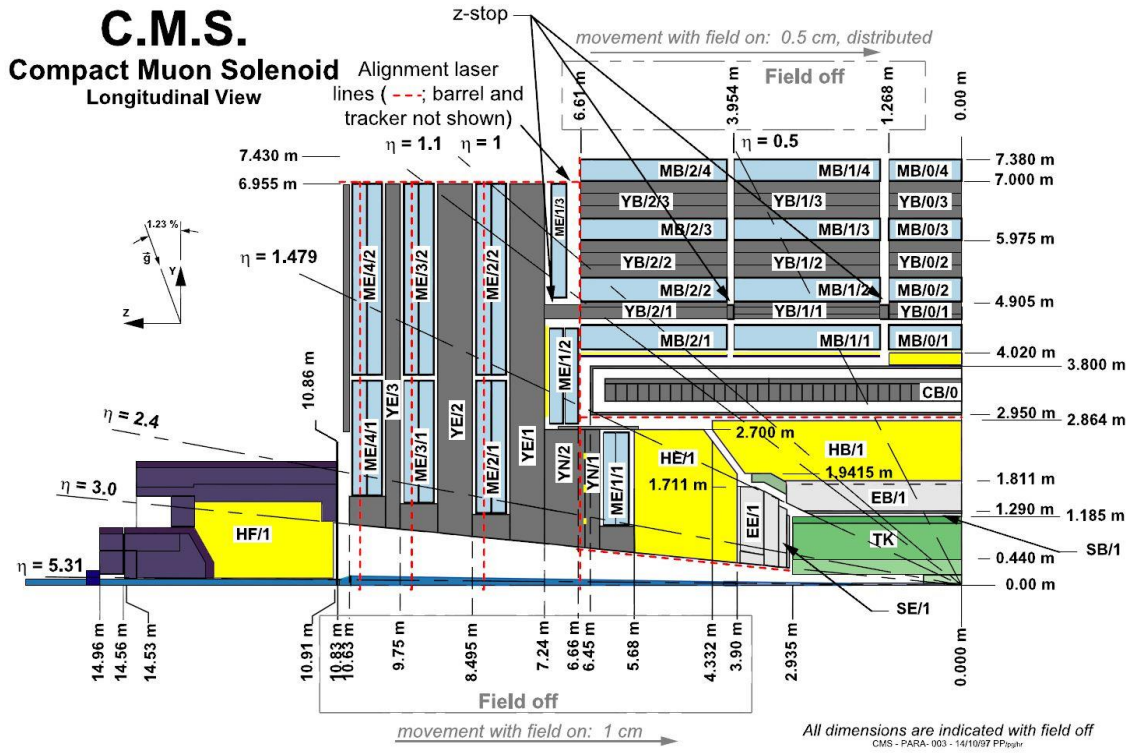


Fig. 1: Longitudinal view of one quadrant of the CMS detector. The positions of the Z-stops are indicated. Laser lines (in dashed) used for the Alignment System are also shown, except for the barrel region.

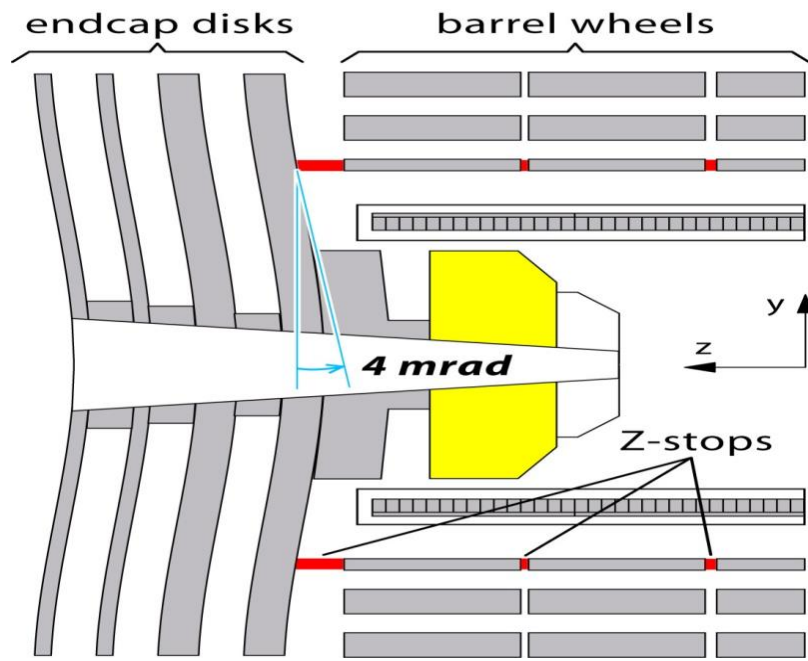
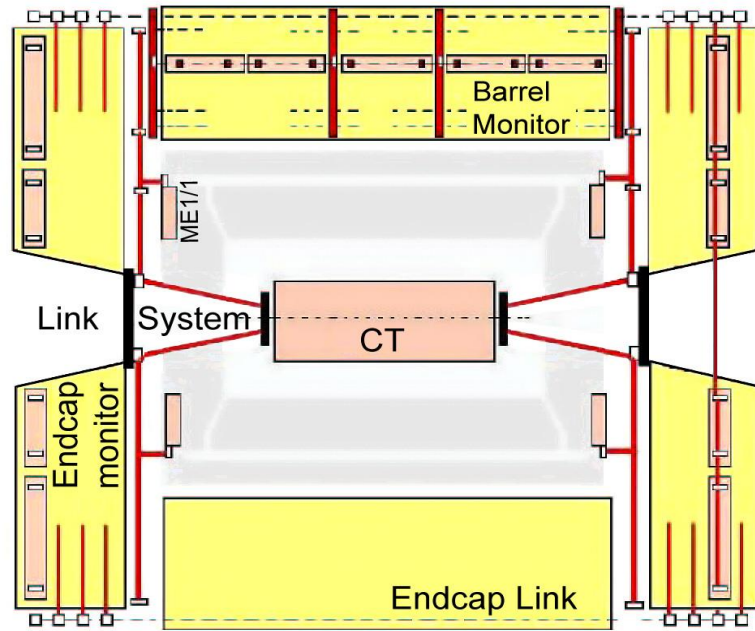


Fig. 2: Sketch of the deformation of the endcap iron disks as a result of the compression due to the magnetic field forces and the resistance of the barrel Z-stops.

a)



b)

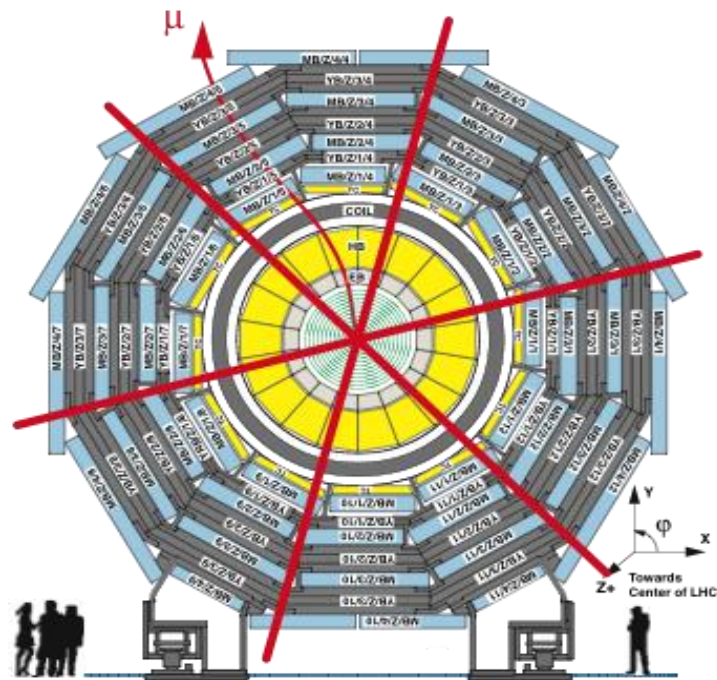


Fig. 3: Schematic view of the Alignment System. a): one Φ alignment plane. The continuous and dotted lines show different optical paths. b): transverse view of the barrel muon detectors. The crossing lines indicate the three alignment Φ planes. The CMS coordinate system is also indicated in the figure.

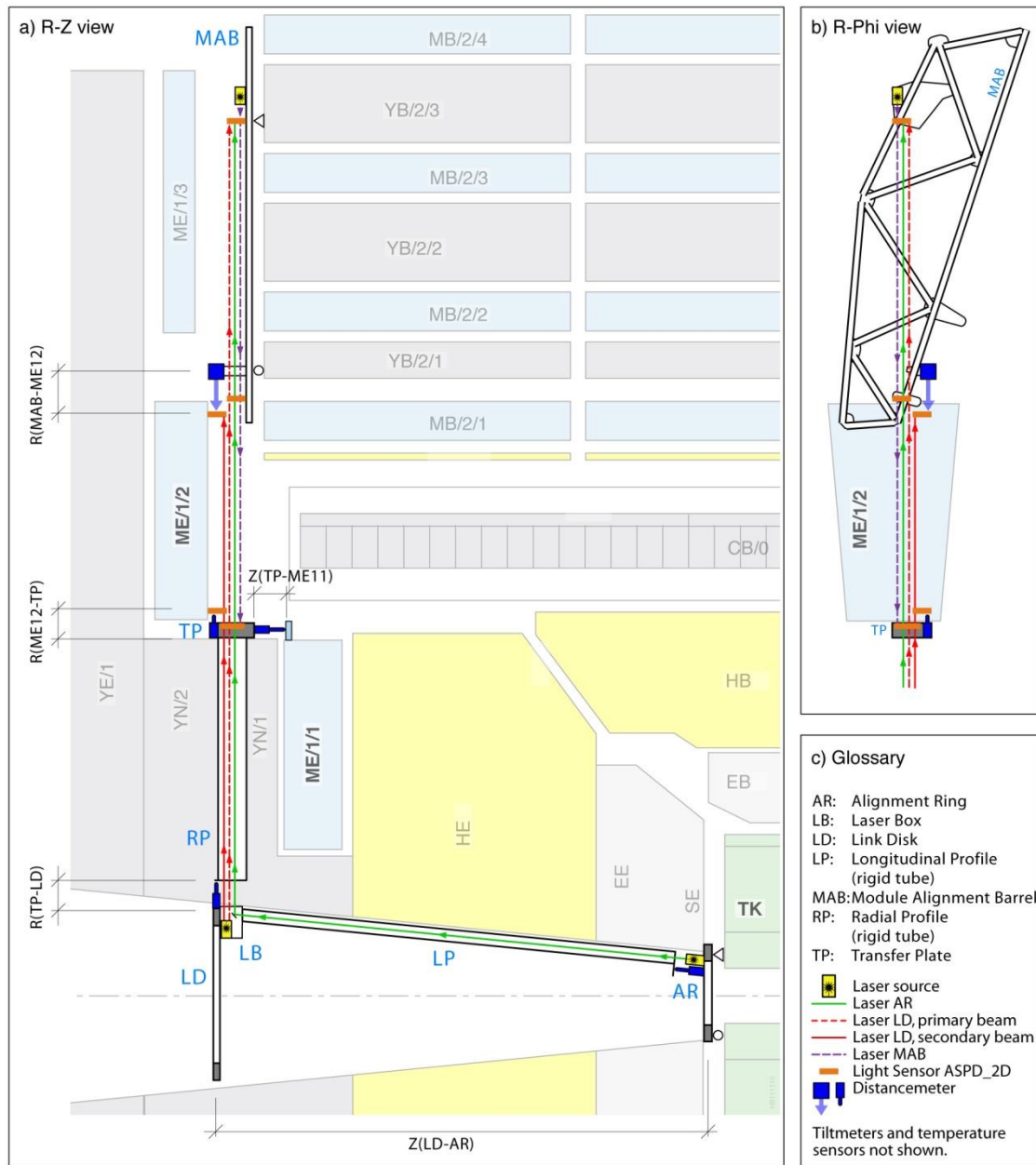


Fig. 4: Sketch of main Link Alignment elements (not to scale) in a quadrant of a Φ plane. The distances whose variations were used to study the evolution of deformations are $R(\text{MAB}-\text{ME1}/2)$, $Z(\text{TP}-\text{ME1}/1)$ and $Z(\text{LD}-\text{AR})$. Tiltmeters and temperature sensors are not shown.

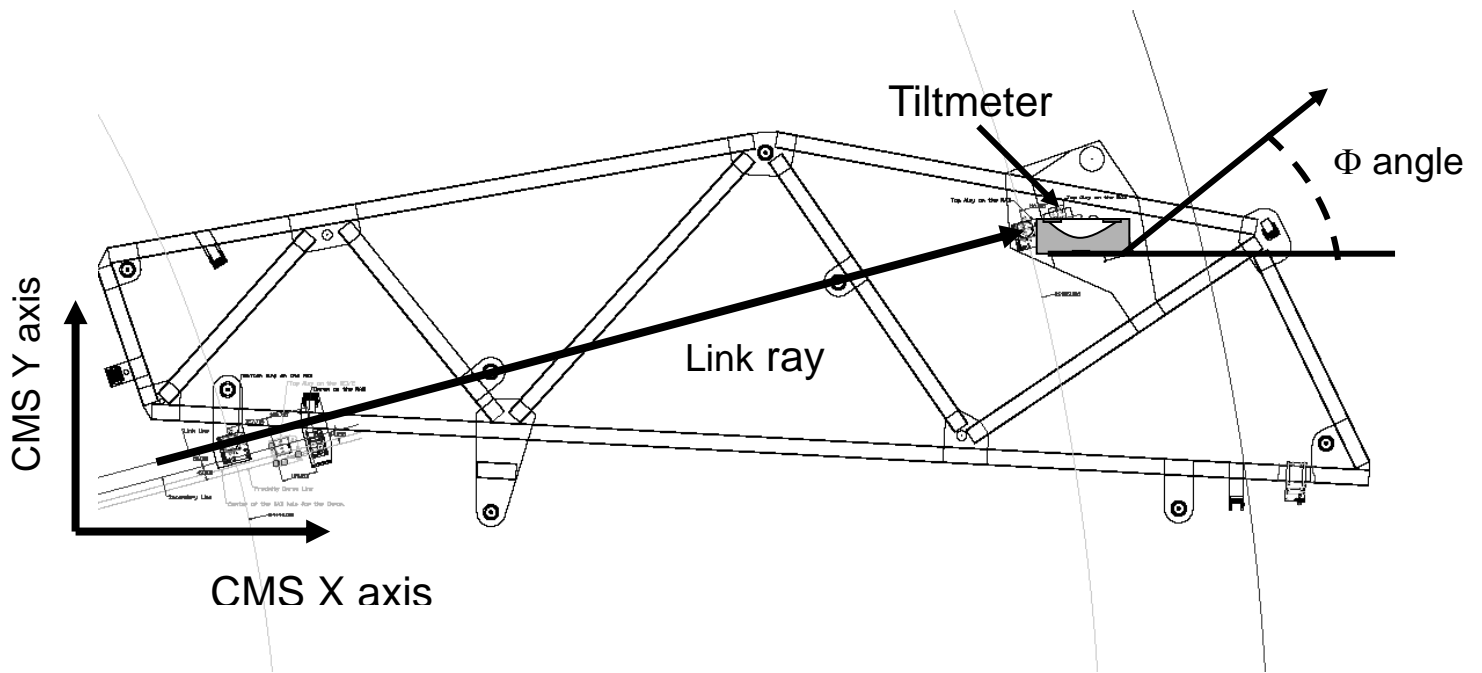


Fig. 5: A MAB structure, showing the position of the tiltmeter for Φ monitoring.

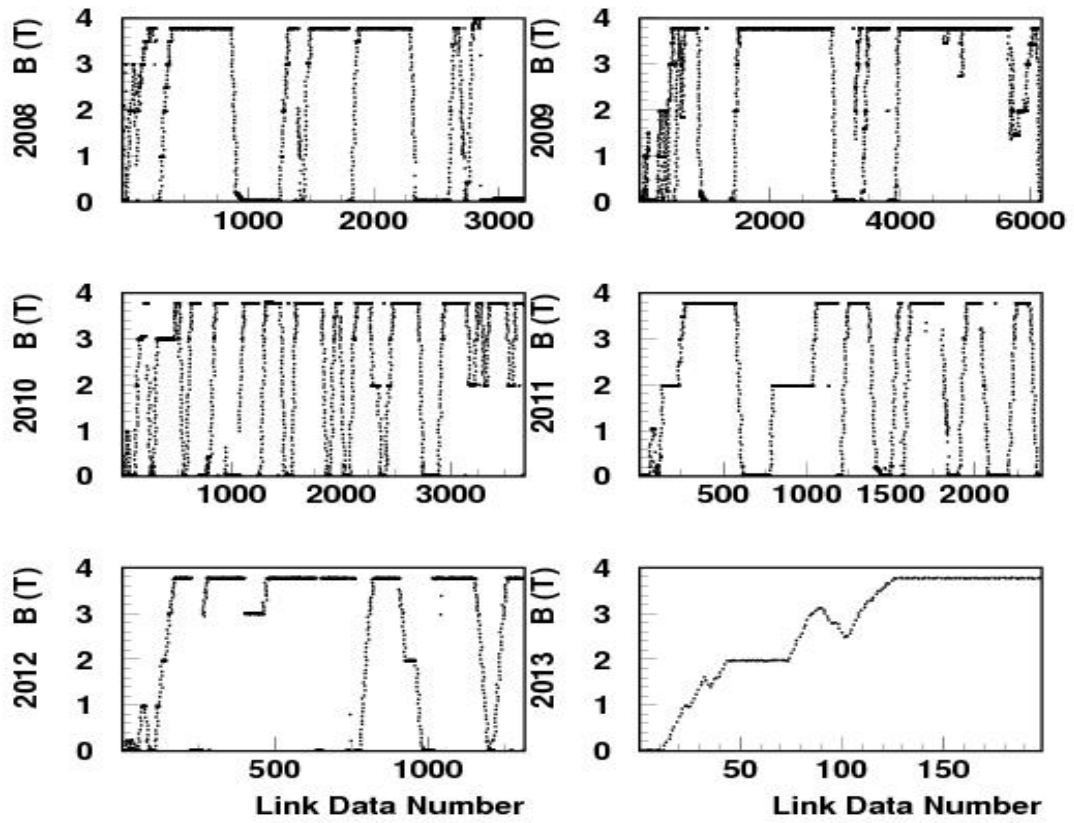


Fig. 6: The CMS magnetic field intensities as a function of the Link data number along the CMS 2008 - 2013 operations.

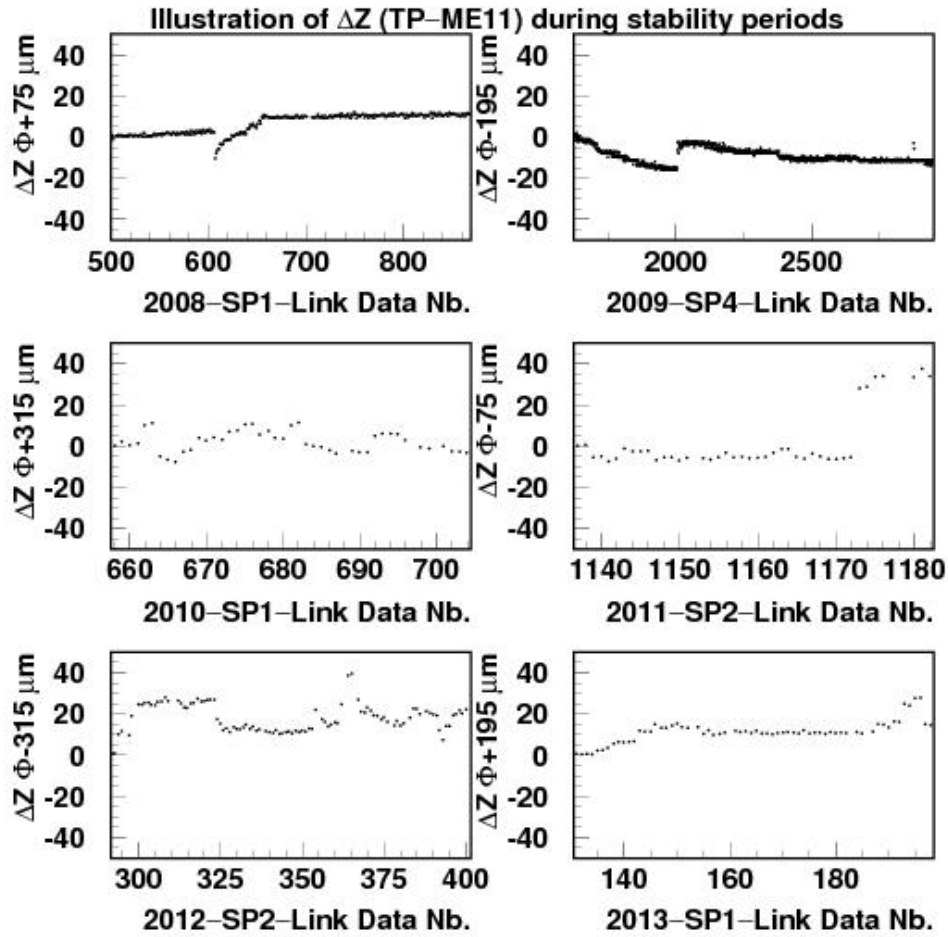


Fig 7: Evolution of the ΔZ (TP-ME11) relative distance (vertical axis, in μm) as a function of the Link Data Number proper to the considered OP-SP data set, for different Φ sectors.

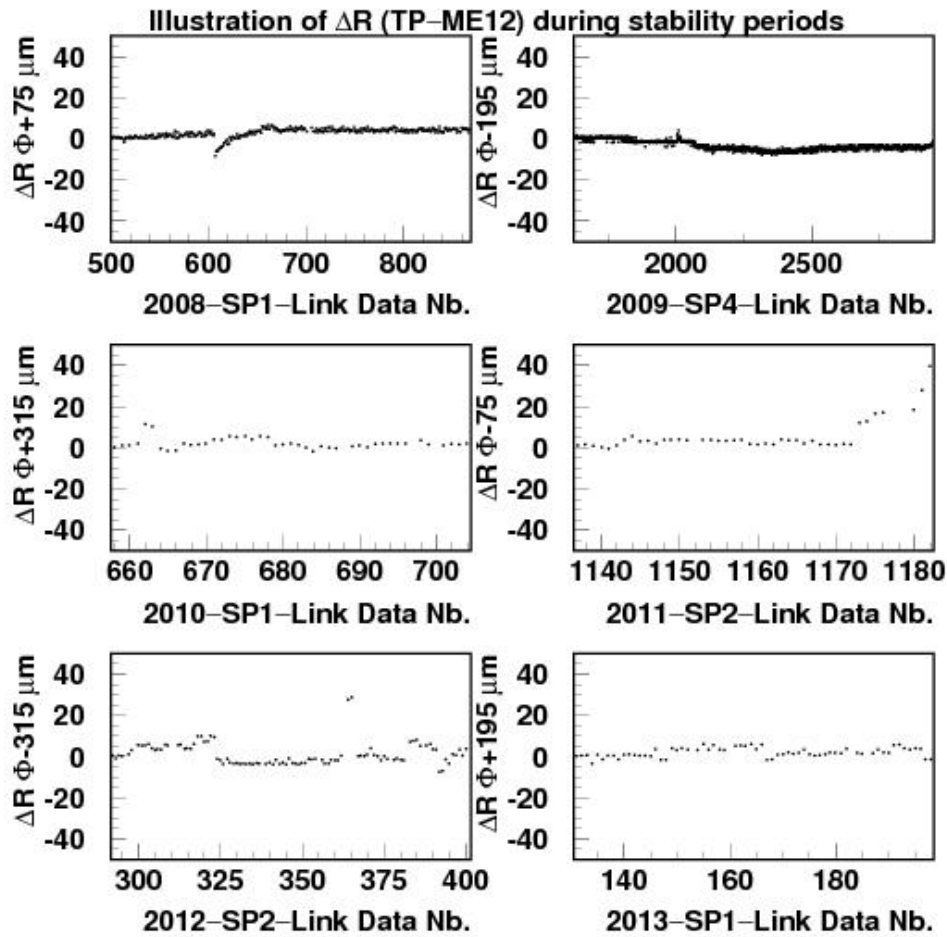


Fig. 8: Evolution the ΔR (TP-ME12) value (vertical axis, in μm) as a function of the Link Data Number proper to the considered data set for the same Φ sectors used to illustrate the ΔZ (TP-ME11) motion on Fig. 7.

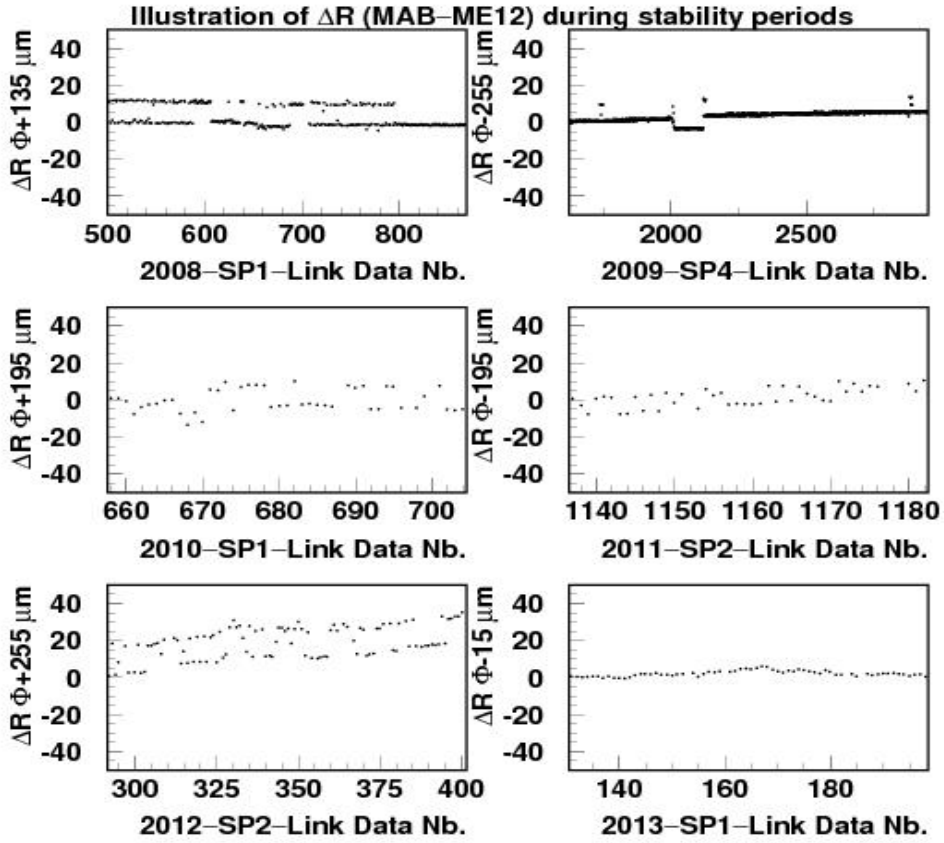


Fig. 9: Relative ΔR (MAB-ME12) radial distance (vertical axis, in μm) as a function of the Link Data number for some Φ sectors at positive and negative CMS Z sides during the considered OY-SP data taking periods. For this illustration we have chosen sectors showing the greatest measured motions.

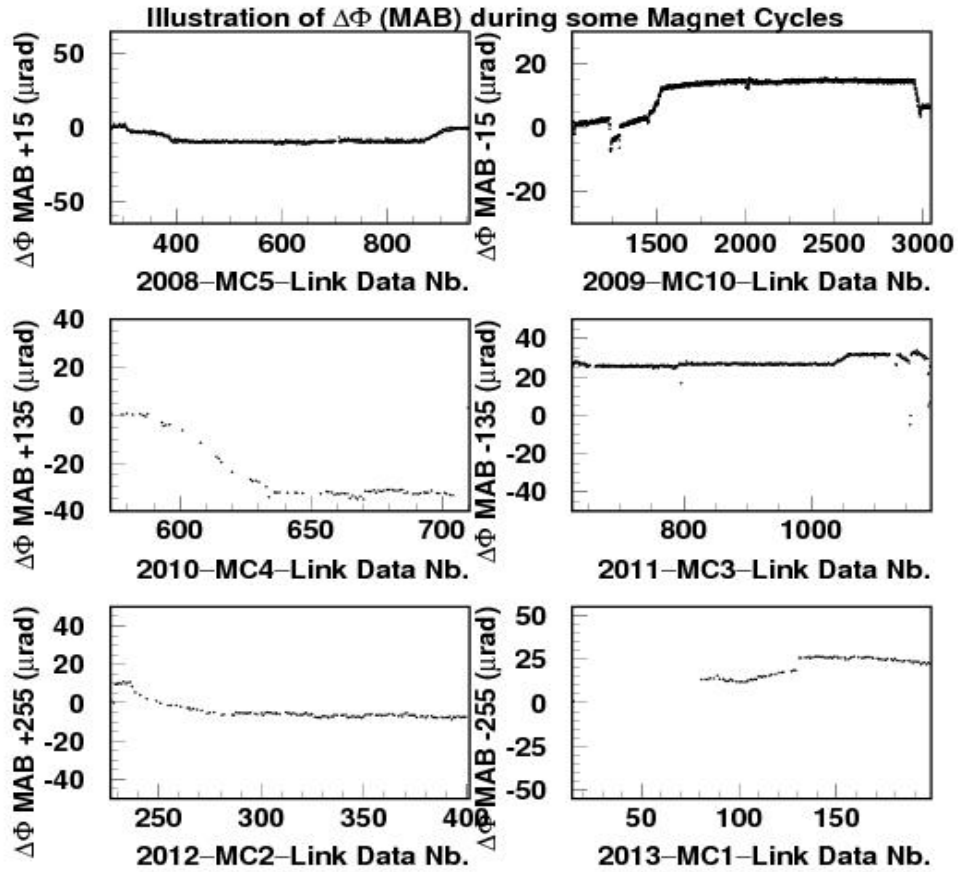


Fig 10: Monitored $\Delta\Phi$ motions (vertical axis, in μrad) for some of the Magnet Cycles (MC) containing the Stability Periods investigated in this document. $\Delta\Phi$ is calculated with respect to the initial inclination of the sensor at $B = 0$ T and it is shown as a function of the Link Data Number of the MC in question.

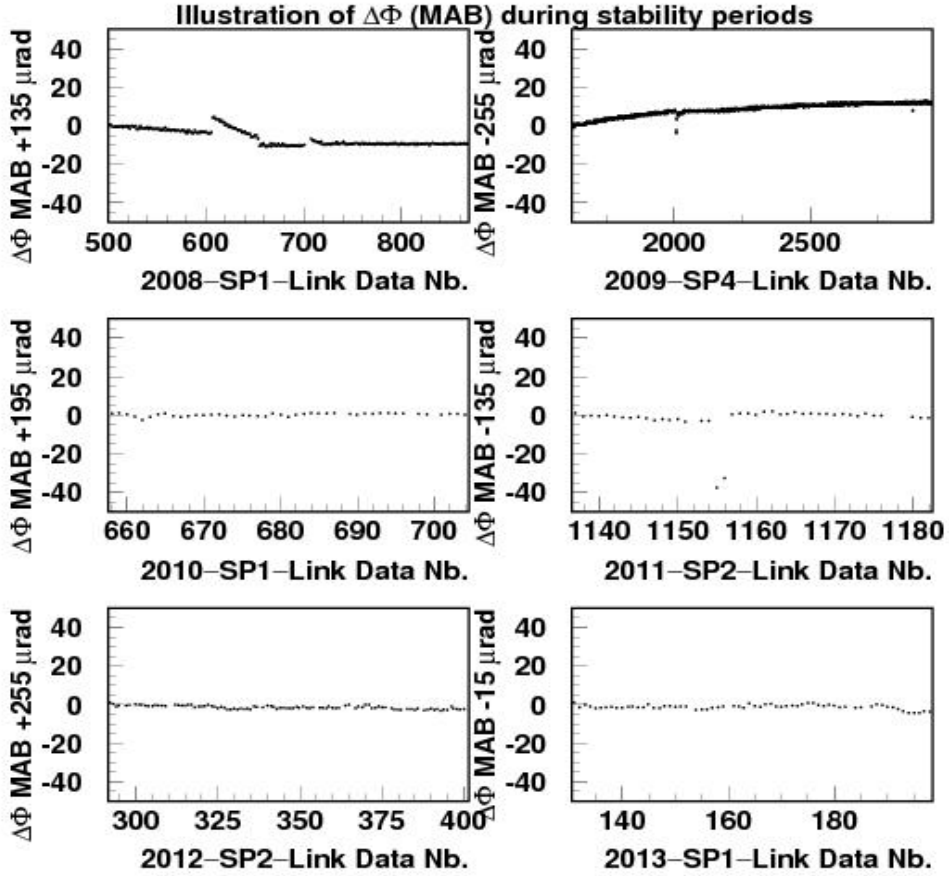


Fig. 11: The reconstructed $\Delta\Phi$ (MAB) rotations (vertical axis, in μrad) as a function of the Link Data number for some Φ sectors at positive and negative CMS Z sides during the considered OY-SP data taking periods. The sensors measuring the eventual tilts have a measured resolution of $\sim 40 \mu\text{rad}$.

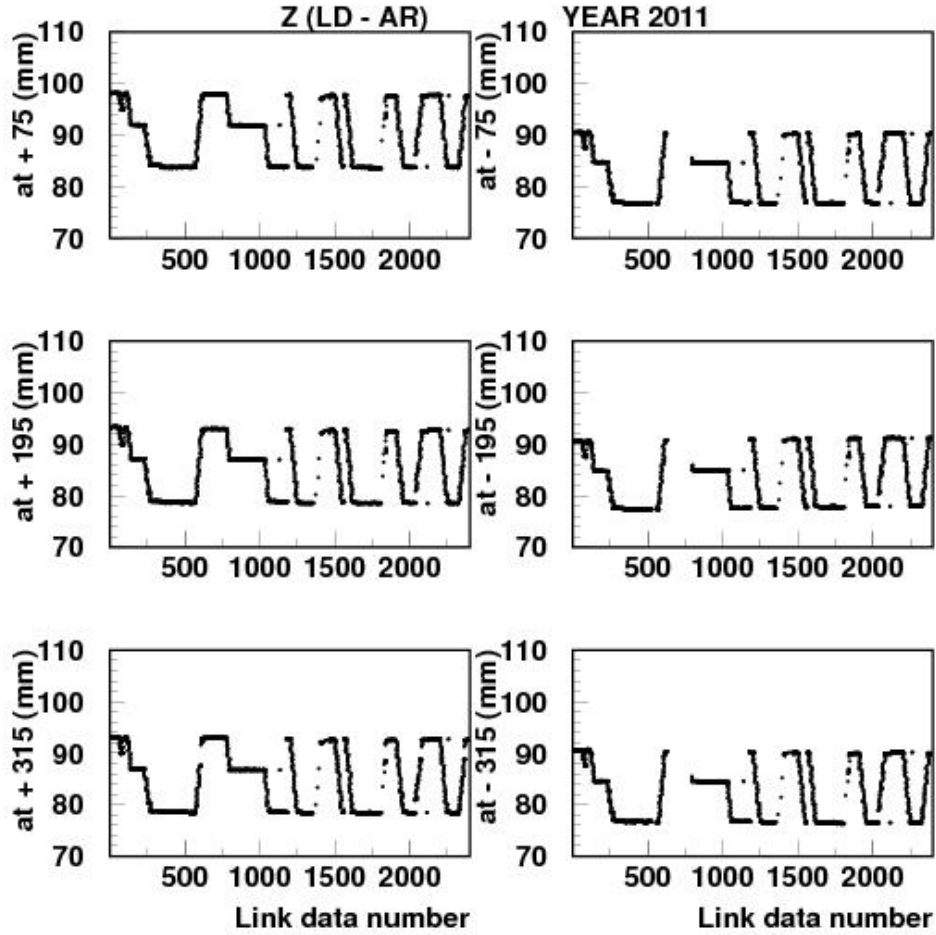


Fig.12: In the vertical axis, the Z (LD-AR) distance during the year 2011, monitored by the Sakae potentiometers at six Φ quadrants ($\pm 75^\circ$, $\pm 195^\circ$ and $\pm 315^\circ$, the sign refers to the CMS Z side) as a function of the link data number. There were 9 magnet cycles (see Table 4).

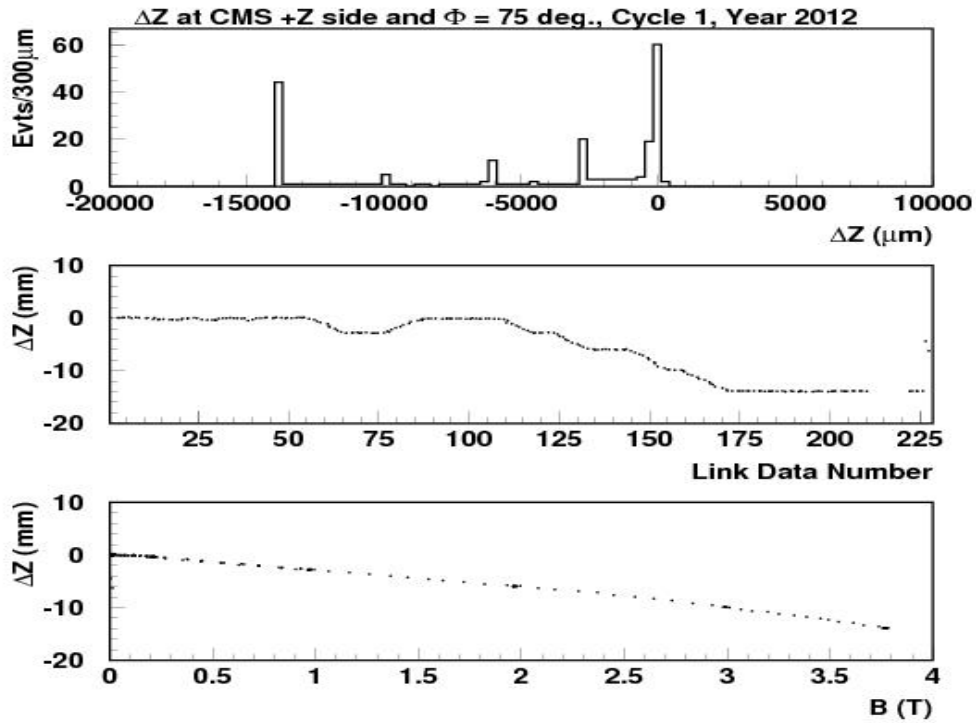


Fig. 13: ΔZ (LD-AR) monitored by the Sakae potentiometer at the $\Phi = +75^\circ$ quadrant, the sign refers to the CMS Z, during the first magnet cycle in 2012 (see Table 5). Top: histogram of data points. The maximum motion registered is -14.99 mm. Middle: ΔZ as a function of the Link Data Number. By the last data $B = 0$ T and LD returns to its initial position. Bottom: ΔZ as a function of the magnetic field intensity showing the expected quadratic behaviour.

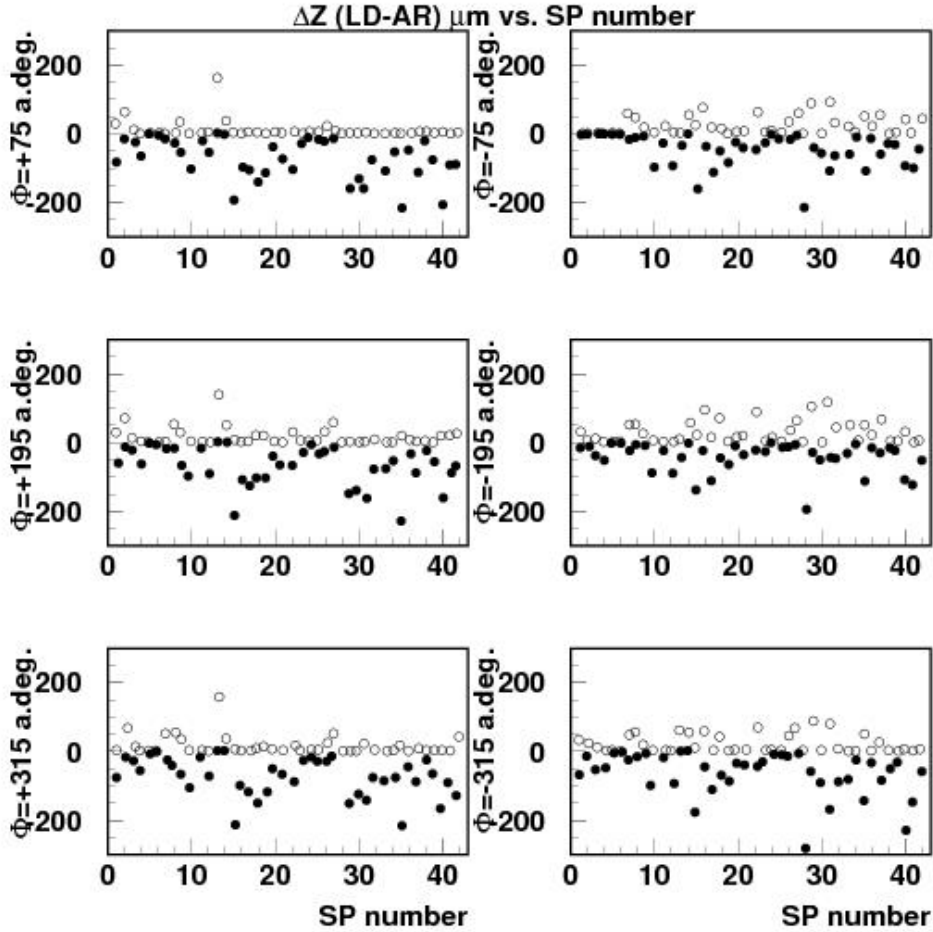


Fig. 14: $\Delta Z(\text{LD-AR})$ monitored by the Sakae potentiometers during the 42 Stability Periods along the 2008 to 2013 CMS years of operation. $\Delta Z(\text{LD-AR}) = Z(\text{LD-AR})_{\text{data-number}} - Z(\text{LD-AR})_{\text{initial}}$, where the initial $Z(\text{LD-AR})$ values are read out at $B = B_{\text{max}}$ (3.8 or 4 T) at the six Φ positions corresponding to the first data taken 24 hours after B_{max} is reached. For each SP the two extreme monitored values registered are shown: the black dots represent the maximum LD-AR approach (negative values) and the open circles correspond to the maximum LD-AR separation in the apparent “accordion” motion.

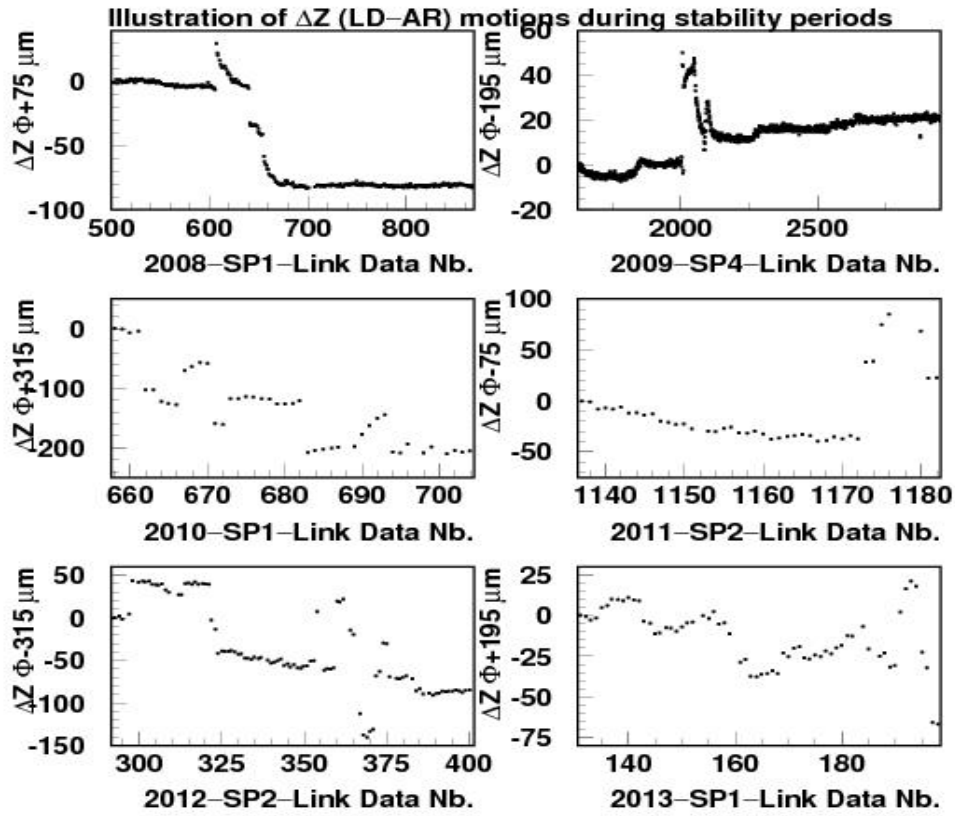


Fig. 15: ΔZ (LD-AR) distance measurements, in microns, for the indicated Φ quadrant (sign refers to + or - Z CMS side) as a function of the Link Data Number during the indicated OY-SP.

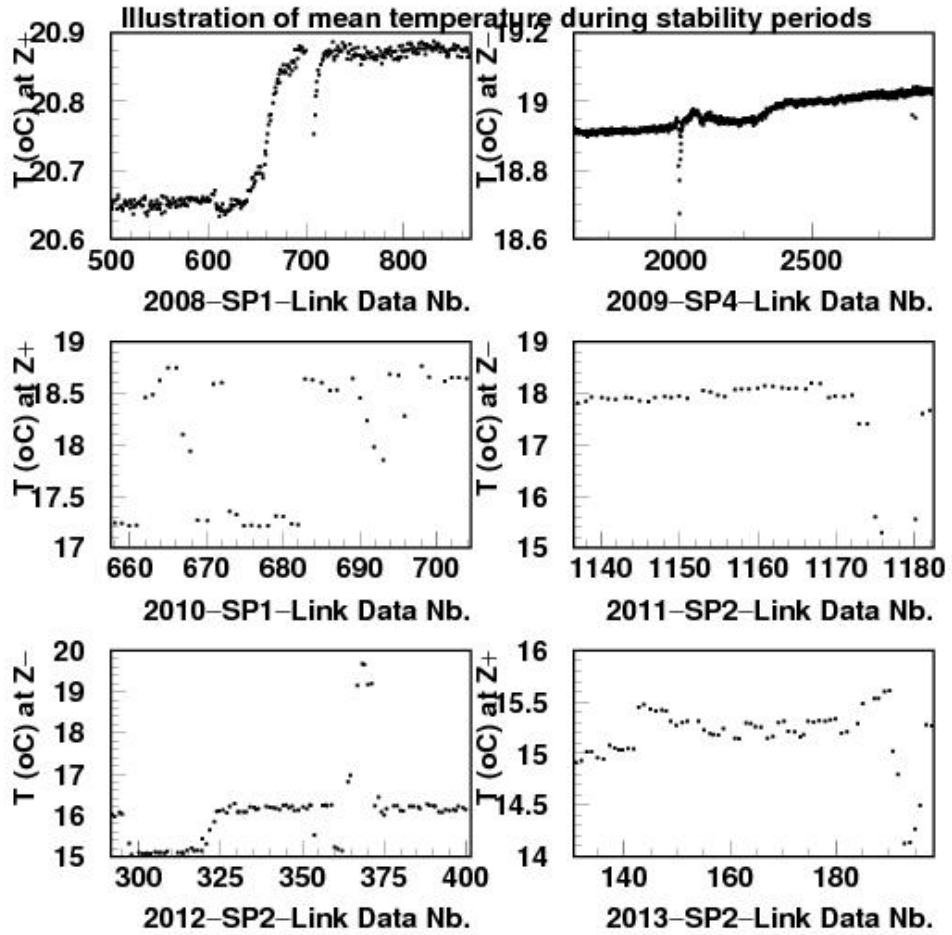


Fig 16: Averaged temperature, in $^{\circ}\text{C}$, in the neighbourhoods of the aluminium profiles for the indicated CMS Z side (sign refers to the side) as a function of the Link Data Number during the mentioned OperationYear–StabilityPeriod data set. There is a one to one correspondence with the Φ quadrants in Fig. 15.

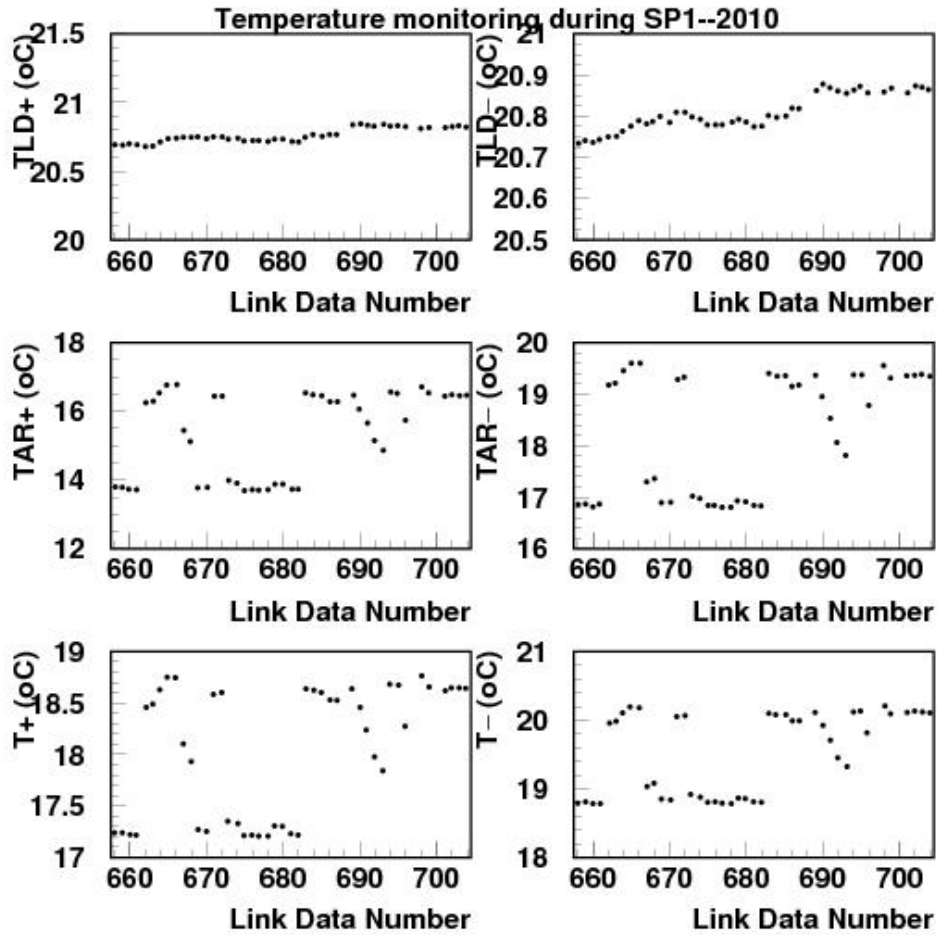


Fig 17: Monitoring of the temperature during the SP1 in year 2010 as a function of the Link Data Number. Data are recorded twice per day. Most of the points represent two measurements superimposed. Left column corresponds to CMS Z+ side, the three plots represent the temperature measured near the Link Disk (6 PT100 sensors), the Alignment Ring (2 PT100 sensors) and the assumed temperature, $T = (TLD + TAR)/2$, in the air volume around the Long Profiles joining the Link Disk to its corresponding Alignment Ring. Right column are the recorded data at the Z- side.

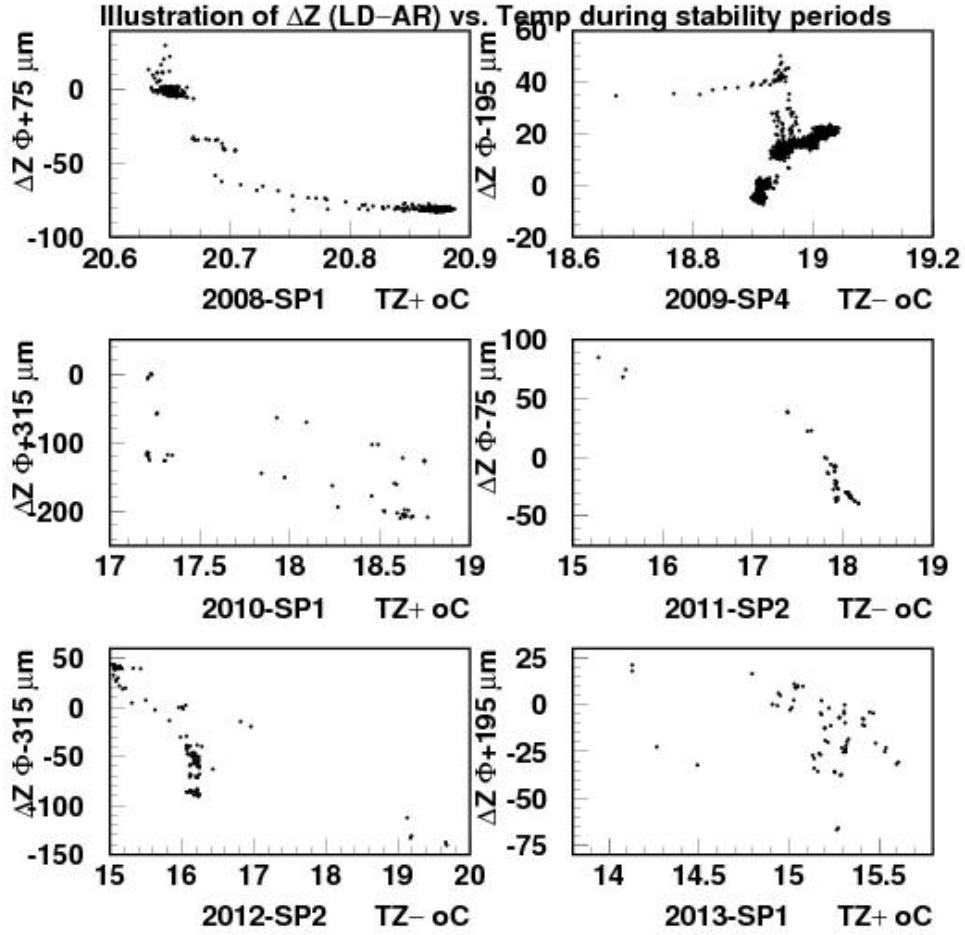


Fig 18: ΔZ (LD-AR) distance measurements, in microns, for the indicated Φ quadrant (sign refers to + or - Z CMS side) versus the average temperature T , in °C, for the indicated CMS Z side (sign refers to the side), during the indicated Stability Period for the mentioned year. Although the correlations exist, their parametrization do not appear to be simple and unique.

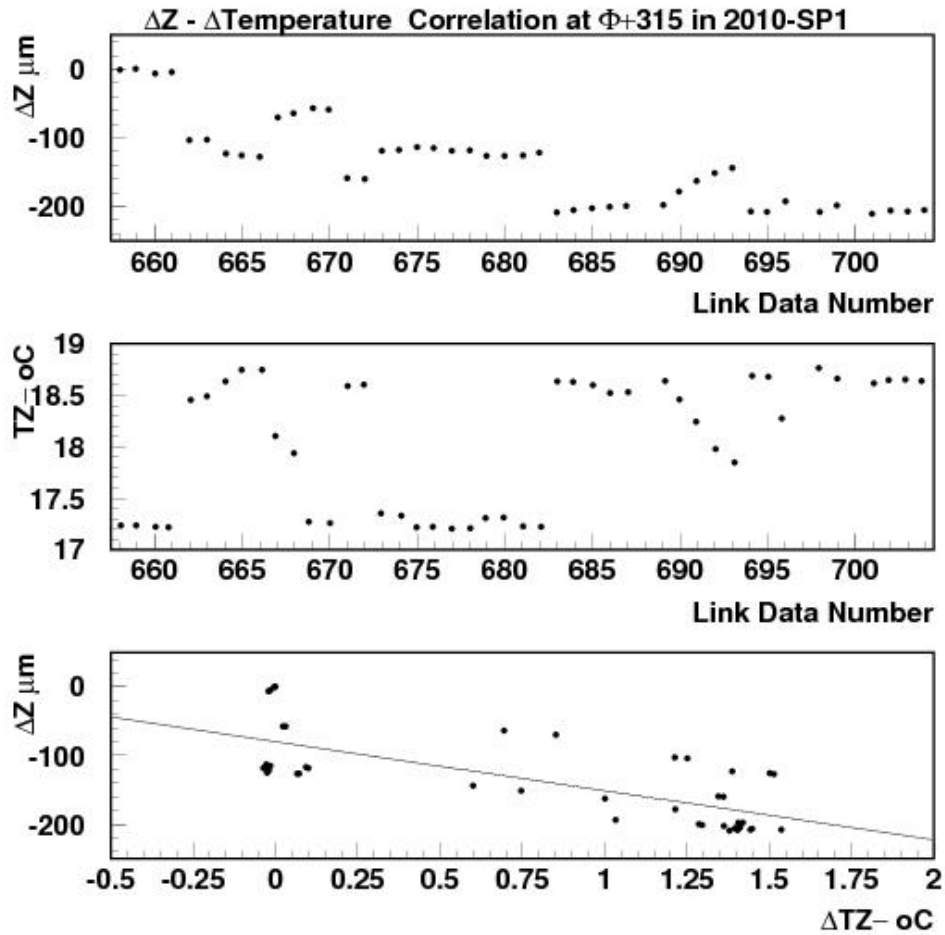


Fig 19: Correlation of the measured ΔZ (LD-AR) with the changes in the temperature in the air volume around the Longitudinal Profiles. In the case of this example the relation between the two measured quantities, with respect to those of the first data taking during the SP1 in the year 2010 at $\Phi = +315$, is $\Delta Z (\mu m) = (-71.6 \pm 9.5) (\mu m/^{\circ}C) \times \Delta T (^{\circ}C)$, with $\chi^2/NDF = 50/42$. $\Delta T = T_{data} (^{\circ}C) - 17.24 (^{\circ}C)$.